Mitigating climate biases in the mid-latitude North Atlantic by increasing model resolution: SST gradients and their relation to blocking and the jet.

Panos Athanasiadis

panos.athanasiadis@cmcc.it

November 2022

cmcc
Centro Euro-Mediterraneo
sui Cambiamenti Climatici

Mitigating Climate Biases in the Midlatitude North Atlantic by Increasing Model Resolution: SST Gradients and Their Relation to Blocking and the Jet

PANOS J. ATHANASIADIS,[a] FUMIAKI OGAWA,[b,c,d] NOUR-EDDINE OMRANI,[b,c] NOEL KEENLYSIDE,[b,c,e] REINHARD SCHIEMANN,[f,g] ALEXANDER J. BAKER,[f,g] PIER LUIGI VIDALE,[f,g] ALESSIO BELLUCCI,[a,h] PAOLO RUGGIERI,[i,a] REIN HAARSMA,[j] MALCOLM ROBERTS,[k] CHRIS ROBERTS,[l] LENKA NOVAK,[m] AND SILVIO GUALDI[a]

[a] *Centro Euro-Mediterraneo sui Cambiamenti Climatici (CMCC), Bologna, Italy*
[b] *University of Bergen, Bergen, Norway*
[c] *Bjerknes Centre for Climate Research, Bergen, Norway*
[d] *Hokkaido University, Sapporo, Japan*
[e] *Nansen Environmental and Remote Sensing Center, Bergen, Norway*
[f] *National Centre for Atmospheric Science Reading, United Kingdom*
[g] *Department of Meteorology, University of Reading, Reading, United Kingdom*
[h] *Istituto di Scienze dell'Atmosfera e del Clima (CNR-ISAC), Bologna, Italy*
[i] *Department of Physics and Astronomy, Alma Mater Studiorum, University of Bologna, Bologna, Italy*
[j] *Royal Netherlands Meteorological Institute (KNMI), De Bilt, Netherlands*
[k] *Met Office, Exeter, United Kingdom*
[l] *European Centre for Medium-Range Weather Forecasts, Reading, United Kingdom*
[m] *Caltech, Pasadena, California*

(Manuscript received 8 July 2021, in final form 29 June 2022)

ABSTRACT: Starting to resolve the oceanic mesoscale in climate models is a step change in model fidelity. This study examines how certain obstinate biases in the midlatitude North Atlantic respond to increasing resolution (from 1° to 0.25° in the ocean) and how such biases in sea surface temperature (SST) affect the atmosphere. Using a multimodel ensemble of historical climate simulations run at different horizontal resolutions, it is shown that a severe cold SST bias in the central North Atlantic, common to many ocean models, is significantly reduced with increasing resolution. The associated bias in the time-mean meridional SST gradient is shown to relate to a positive bias in low-level baroclinicity, while the cold SST bias causes biases also in static stability and diabatic heating in the interior of the atmosphere. The changes in baroclinicity and diabatic heating brought by increasing resolution lead to improvements in European blocking and eddy-driven jet variability. Across the multimodel ensemble a clear relationship is found between the climatological meridional SST gradients in the broader Gulf Stream Extension area and two aspects of the atmospheric circulation: the frequency of high-latitude blocking and the southern-jet regime. This relationship is thought to reflect the two-way interaction (with a positive feedback) between the respective oceanic and atmospheric anomalies. These North Atlantic SST anomalies are shown to be important in forcing significant responses in the midlatitude atmospheric circulation, including jet variability and the storm track. Further increases in oceanic and atmospheric resolution are expected to lead to additional improvements in the representation of Euro-Atlantic climate.

Posing the problem

- How do North Atlantic SST biases change with increasing resolution in a multi-model framework?
- Does increasing model resolution bring improvements in the representation of North Atlantic blocking and the eddy-driven jet?
- What is the role of reduced SST biases for such improvements in blocking and the jet?

Lee, R.W., Woollings, T.J., Hoskins, B.J. et al. Impact of Gulf Stream SST biases on the global atmospheric circulation. Clim Dyn 51, 3369–3387 (2018).

"The role of this SST bias is examined with a focus on the tropospheric response by performing three sensitivity experiments. The SST biases are imposed on the atmosphere-only configuration of the model over a small and medium section of the Gulf Stream, and also the wider North Atlantic."

"Imposing this warm SST bias here acts to shift and change the strength of the SST gradients in the Gulf Stream which have been shown to be important to ocean– atmosphere interactions (e.g. Parfitt et al. 2016)."

"...reducing ocean and SST biases in these regions of high ocean–atmosphere interaction may also reduce some of the global atmospheric biases in coupled global climate models."

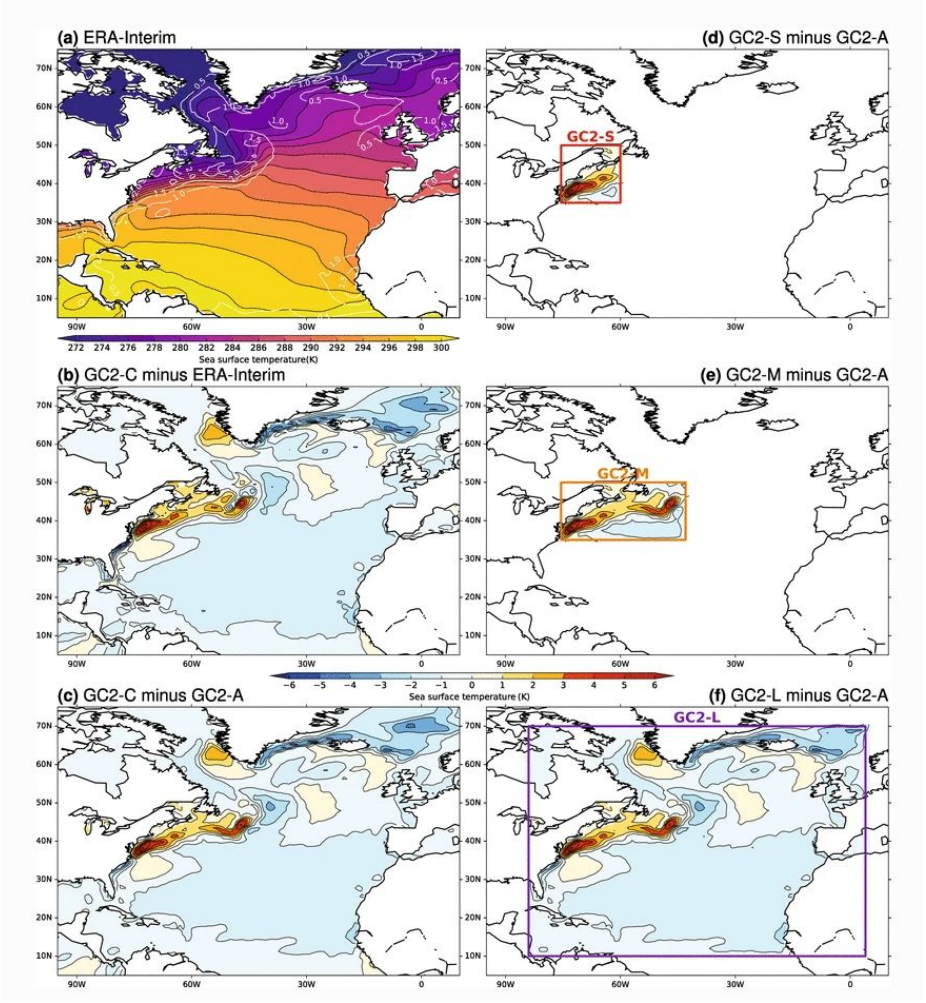

Time mean sea surface temperatures (shading, units: K) in **a** ERA-Interim, **b** GC2-C minus ERA-Interim, **c** GC2-C minus GC2-A, and sensitivity experiments **d** GC2-S minus GC2-A from the small red box region, **e** GC2-M minus GC2-A from the medium orange box region, and **f** GC2-L minus GC2-A from the large purple box region. Monthly frequency standard deviation of ERA-Interim is shown in **a** (white line contours, units: K). Zero differences in **d**–**f** are shown in white

SST bias

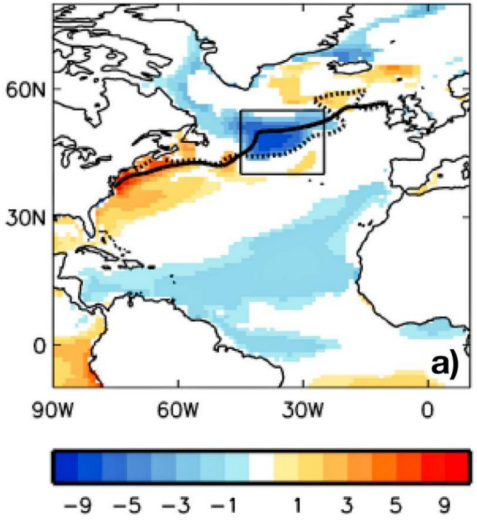

zonal wind bias 60°W–10°E

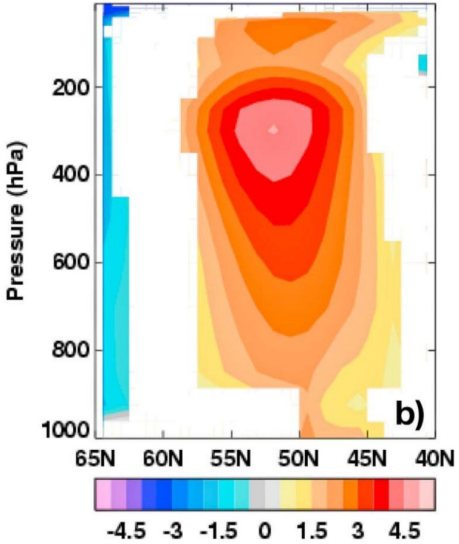

Scaife, A. A., Copsey, D., Gordon, C., Harris, C., Hinton, T., Keeley, S., O'Neill, A., Roberts, M., and Williams, K. (2011):

Improved Atlantic winter blocking in a climate model. *GRL*.

"At standard resolution, our climate model shows the usual error of a large deficit in Atlantic winter blocking frequency. At moderately higher resolution the error is largely removed. Artificially removing the mean bias in the standard model shows that this bias is immediately responsible for the blocking error, as in previous studies. Atmosphere only experiments confirm that SST errors generate much of the westerly bias and the blocking deficit. Additional experiments with ocean-only models demonstrate that ocean model resolution in turn plays a key role in alleviating the SST error."

Keeley, S.P.E., Sutton, R.T. and Shaffrey, L.C. (2012):

The impact of North Atlantic sea surface temperature errors on the simulation of North Atlantic European region climate. *Q.J.R.Met.Soc.*

"The work also suggests that errors in the coupled model storm tracks and North Atlantic Oscillation, compared to reanalysis data, can also be explained partly by these SST errors. Our results suggest that both the error in the Gulf Stream separation location and the path of the North Atlantic Current around the Grand Banks play important roles in affecting the atmospheric circulation."

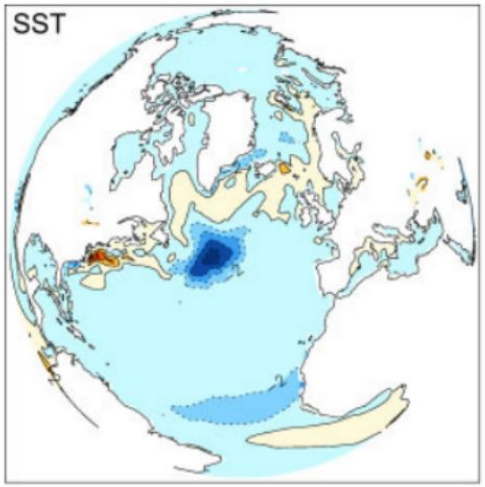

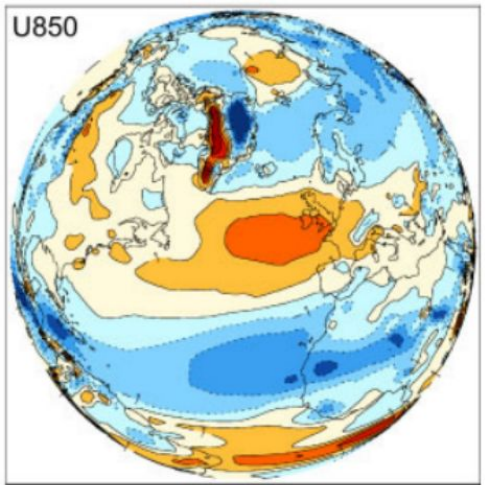

PRIMAVERA HighResMIP models (historical coupled simulations 1950–2014)

No.	Model	Atm. grid (km)	Ocean grid (km)	LR / HR	LOW / HIGH
1	AWI-CM-1-1-LR	129	50	LR	–
2	AWI-CM-1-1-HR	67	25	HR	–
3	CMCC-CM2-HR4	64	25	LR	LOW-RES
4	CMCC-CM2-VHR4	18	25	HR	HIGH-RES
5	CNRM-CM6-1	142	100	LR	LOW-RES
6	CNRM-CM6-1-HR	50	25	HR	HIGH-RES
7	EC-Earth3P	71	100	LR	LOW-RES
8	EC-Earth3P-HR	36	25	HR	HIGH-RES
9	ECMWF-IFS-LR	50	100	LR	LOW-RES
10	ECMWF-IFS-MR	50	25	HR	HIGH-RES
11	ECMWF-IFS-HR	25	25	HR	–
12	HadGEM3-GC31-LL	135	100	LR	LOW-RES
13	HadGEM3-GC31-MM	60	25	HR	HIGH-RES
14	HadGEM3-GC31-HM	25	25	HR	–
15	HadGEM3-GC31-HH	25	8	HR	HIGH-RES
16	MPI-ESM1-2-HR	67	40	LR	LOW-RES
17	MPI-ESM1-2-XR	34	40	HR	HIGH-RES

Biases are assessed against HadISST2 for SSTs and ECMWF reanalyses for blocking.

PRIMAVERA HighResMIP models (historical coupled simulations 1950–2014)

No.	Model	Atm. grid (km)	Ocean grid (km)	LR / HR	LOW / HIGH
1	AWI-CM-1-1-LR	129	50	LR	–
2	AWI-CM-1-1-HR	67	25	HR	–
3	CMCC-CM2-HR4	64	25	LR	LOW-RES
4	CMCC-CM2-VHR4	18	25	HR	HIGH-RES
5	CNRM-CM6-1	142	100	LR	LOW-RES
6	CNRM-CM6-1-HR	50	25	HR	HIGH-RES
7	EC-Earth3P	71	100	LR	LOW-RES
8	EC-Earth3P-HR	36	25	HR	HIGH-RES
9	ECMWF-IFS-LR	50	100	LR	LOW-RES
10	ECMWF-IFS-MR	50	25	HR	HIGH-RES
11	ECMWF-IFS-HR	25	25	HR	–
12	HadGEM3-GC31-LL	135	100	LR	LOW-RES
13	HadGEM3-GC31-MM	60	25	HR	HIGH-RES
14	HadGEM3-GC31-HM	25	25	HR	–
15	HadGEM3-GC31-HH	25	8	HR	HIGH-RES
16	MPI-ESM1-2-HR	67	40	LR	LOW-RES
17	MPI-ESM1-2-XR	34	40	HR	HIGH-RES

Biases are assessed against HadISST2 for SSTs and ECMWF reanalyses for blocking.

Absolute bias reduction

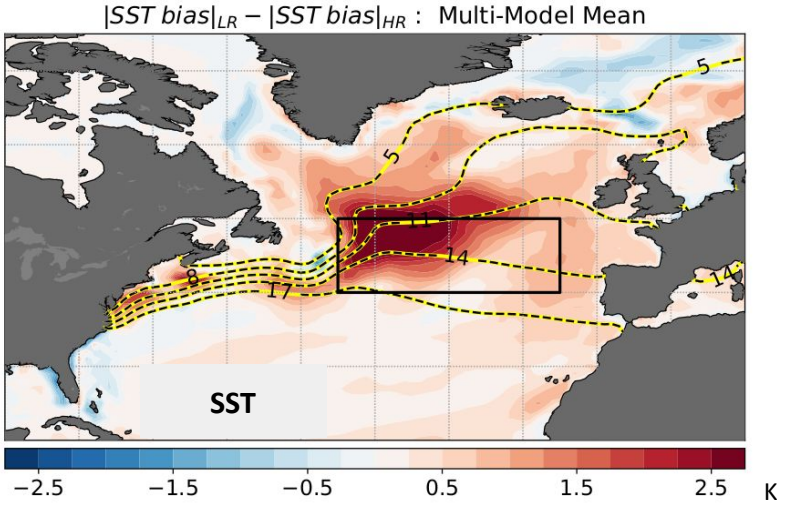

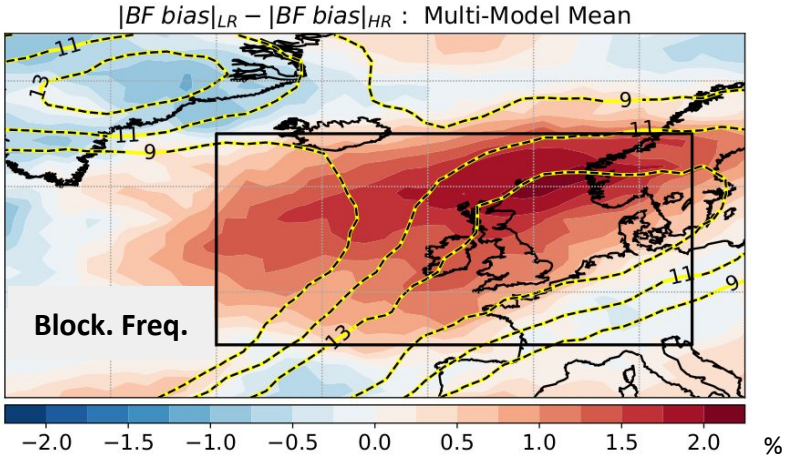

Comparing Biases

LOW-RES **HIGH-RES**

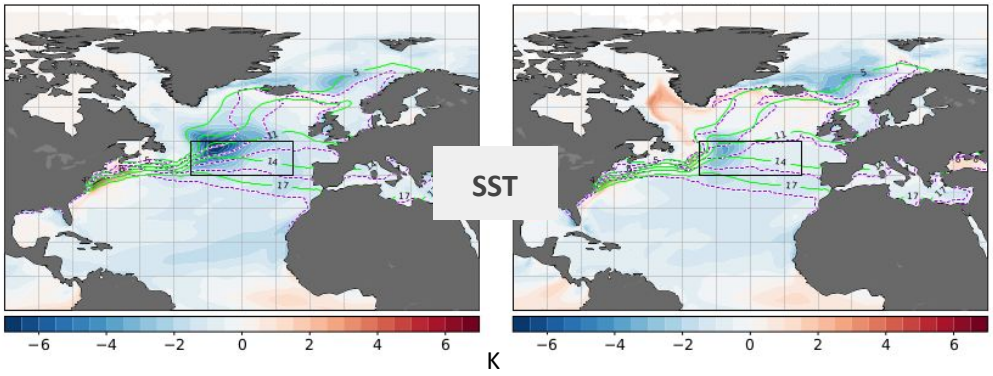

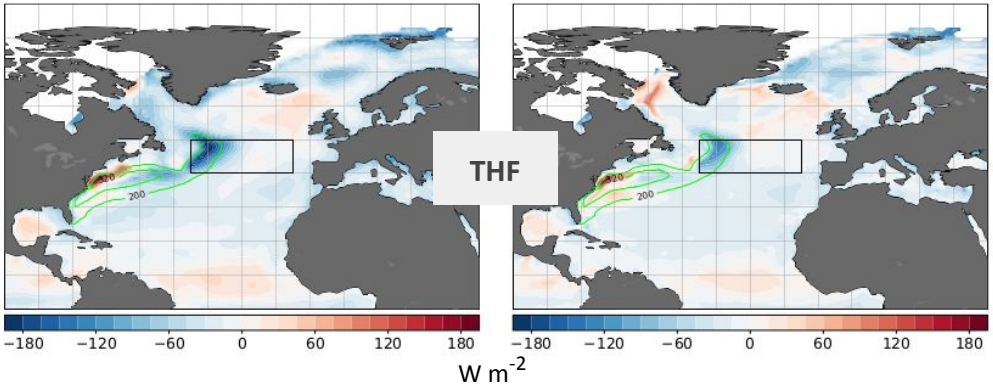

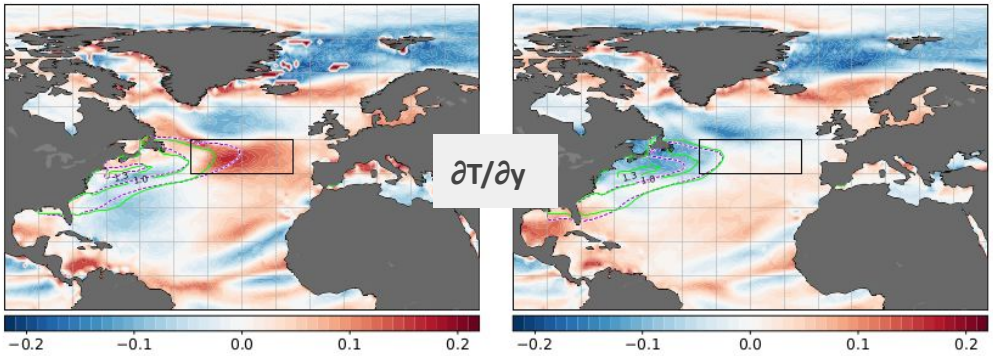

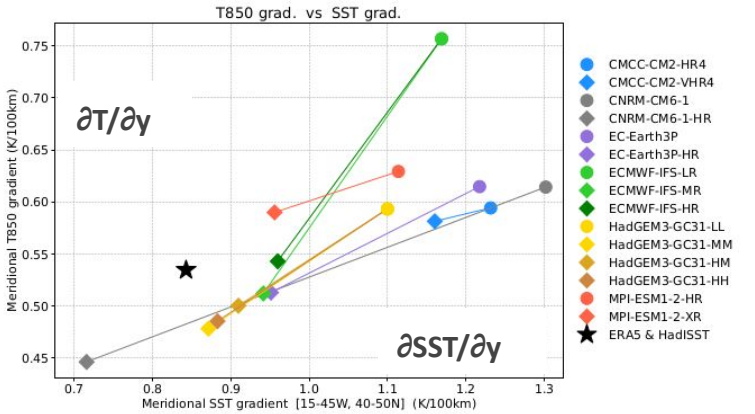

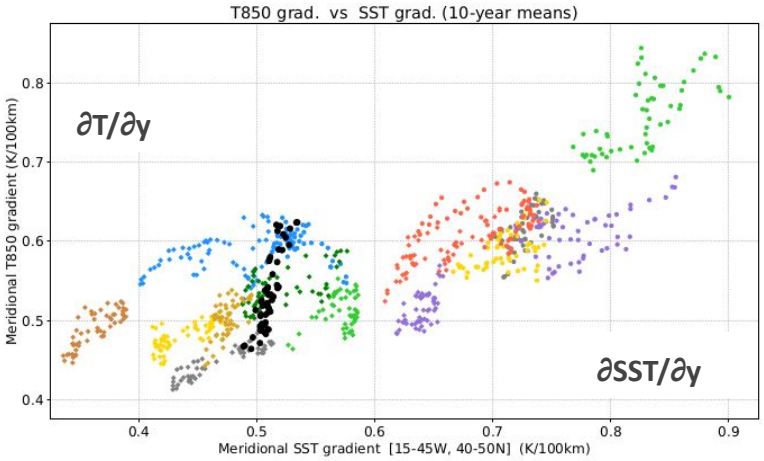

Biases are assessed against OAFlux for surf. fluxes and against ERA5 for the atmospheric fields.

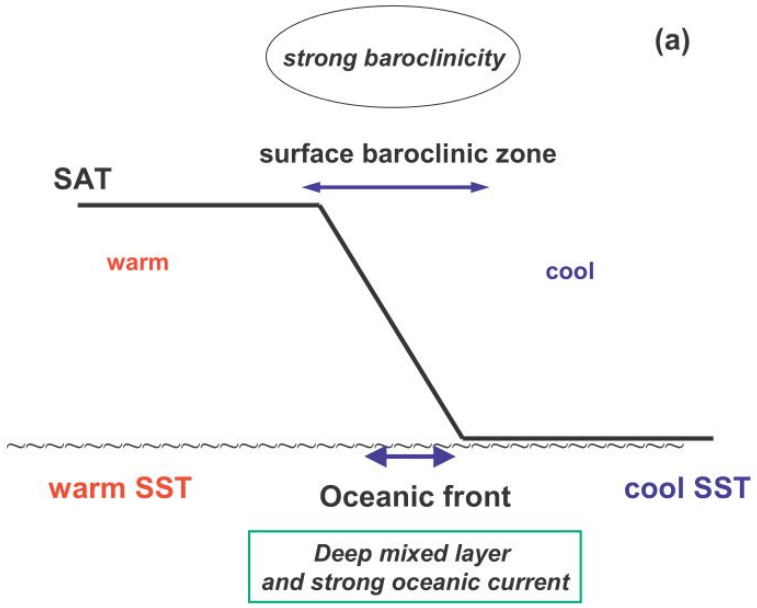

Schematic diagrams showing the restoration of near-surface baroclinicity by an oceanic front through surface sensible heat flux from the ocean against the relaxation by eddy heat transport. **(a)** A strong SAT gradient formed above an oceanic front favors baroclinic eddy growth. **(b)** Poleward eddy heat flux relaxes the SAT gradient and then heat flux from the ocean corresponding to the air–sea temperature difference acts to restore the SAT gradient.

Sampe et al., 2010.

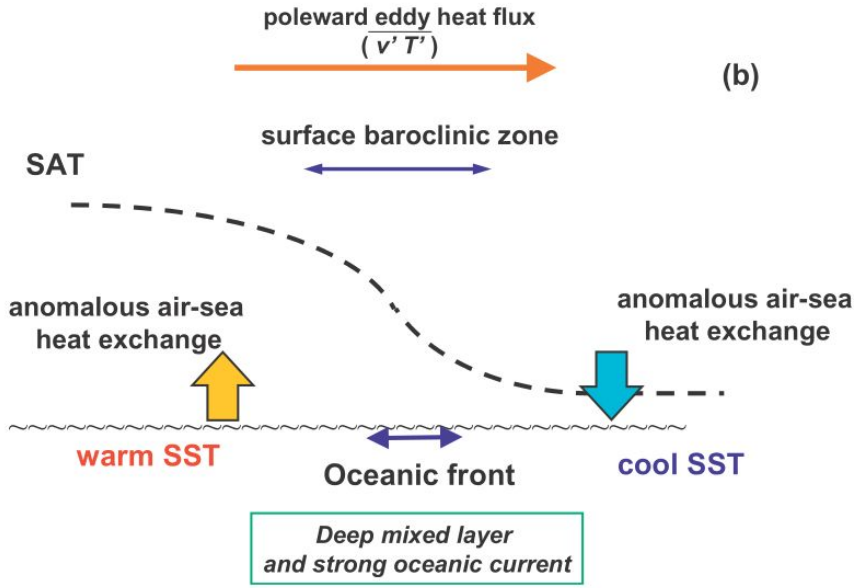

Comparing Biases

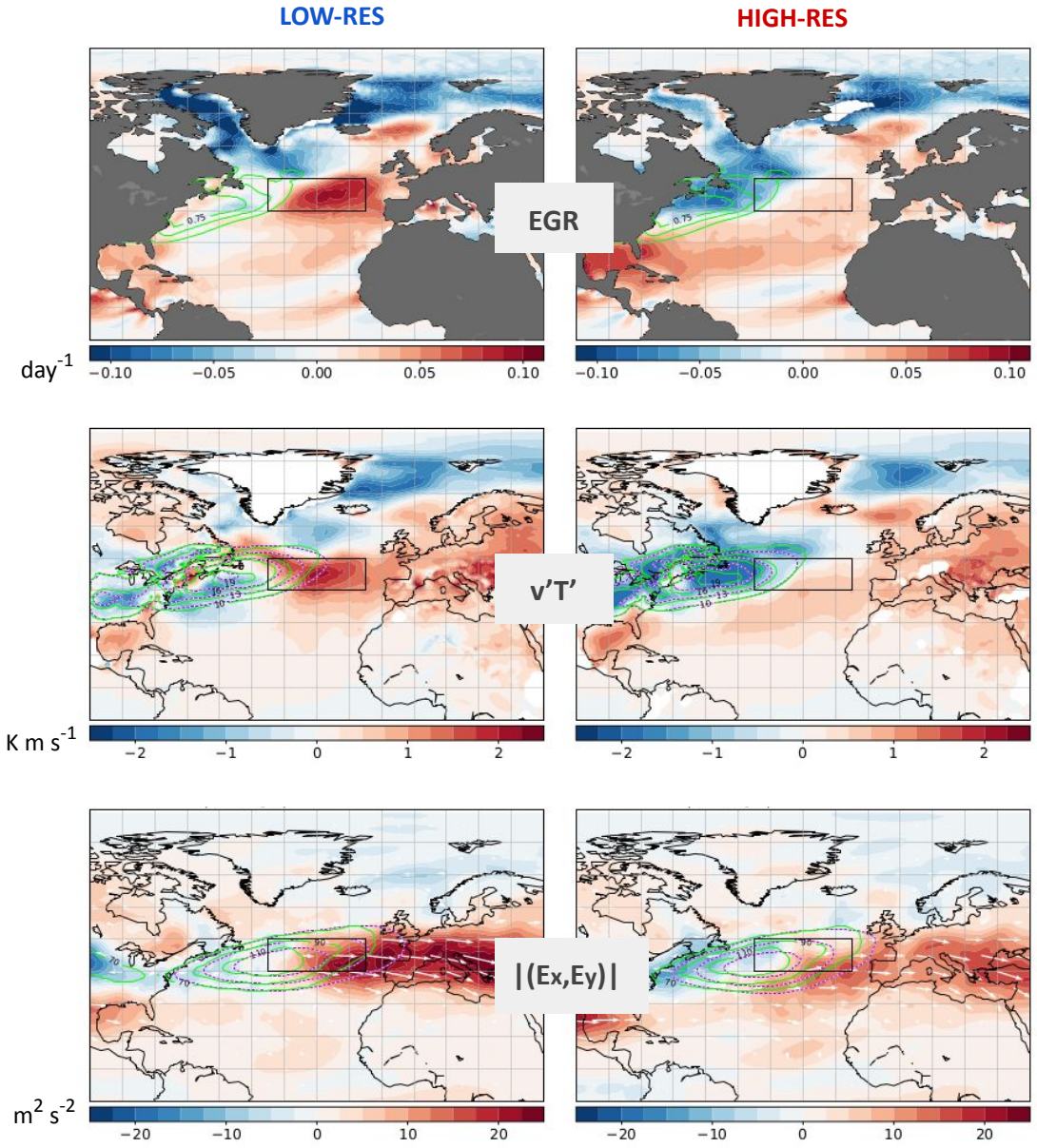

Maximum Eady growth rate

Meridional eddy heat flux by synoptic transients

Horizontal E-vectors

Comparing Biases

LOW-RES HIGH-RES

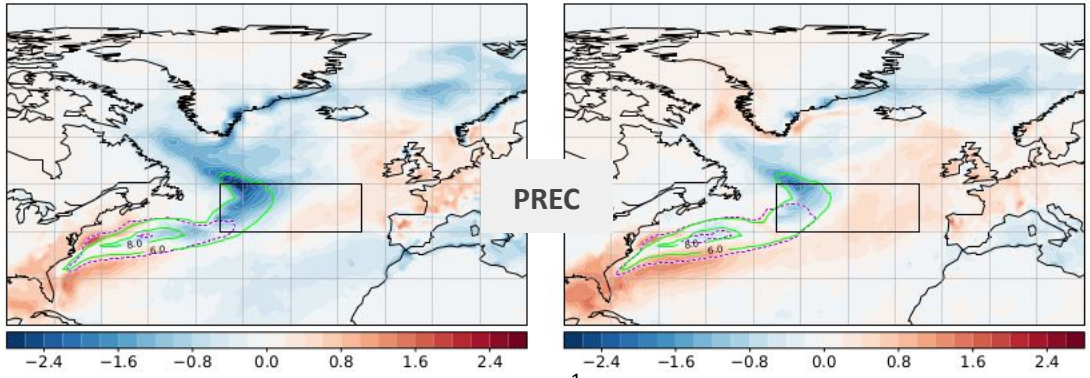

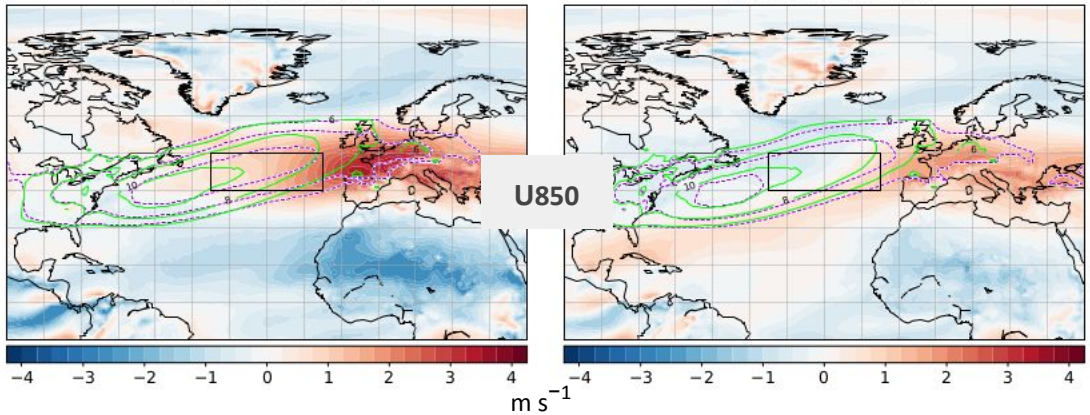

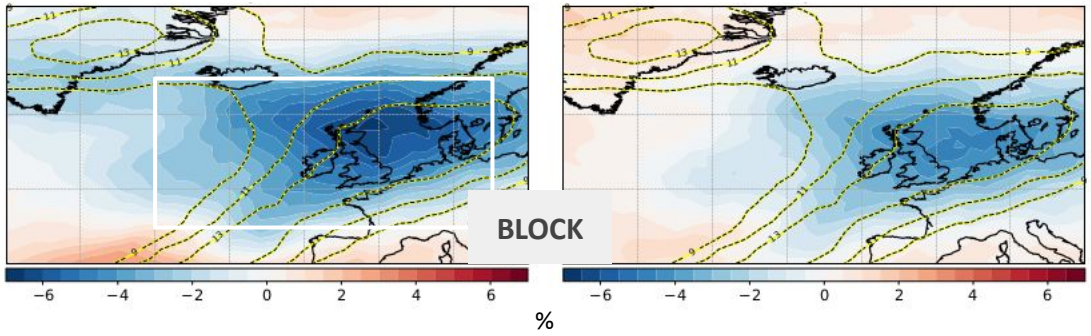

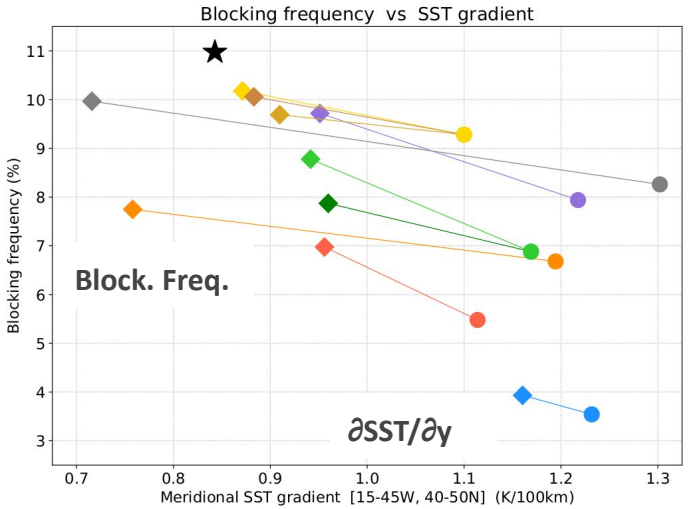

- AWI-CM-LR
- AWI-CM-HR
- CMCC-CM2-HR4
- CMCC-CM2-VHR4
- CNRM-CM6-1
- CNRM-CM6-1-HR
- EC-Earth3P
- EC-Earth3P-HR
- ECMWF-IFS-LR
- ECMWF-IFS-MR
- ECMWF-IFS-HR
- HadGEM3-GC31-LL
- HadGEM3-GC31-MM
- HadGEM3-GC31-HM
- HadGEM3-GC31-HH
- MPI-ESM1-2-HR
- MPI-ESM1-2-XR
- ERA-JOINT & HadISST

Precipitation biases are assessed against ERA5.

Climatologies vary little between different realizations
(results largely insensitive to internal variability)

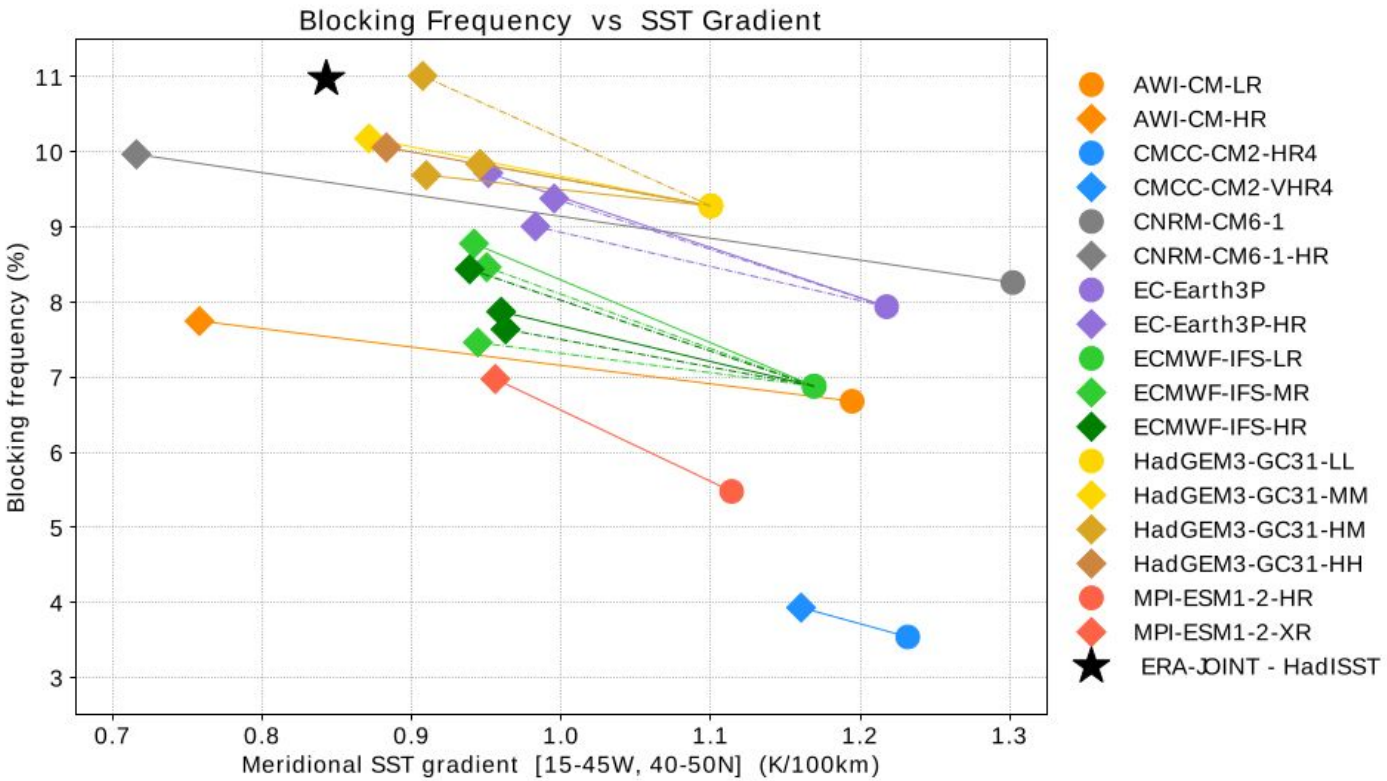

Oceanic origins for wintertime Euro-Atlantic blocking

Ayako Yamamoto[1,2], Masami Nonaka[1], Patrick Martineau[1,2], Akira Yamazaki[1], Young-Oh Kwon[3], Hisashi Nakamura[1,2], and Bunmei Taguchi[4]

[1]Japan Agency for Marine-Earth Science and Technology (JAMSTEC), Yokohama, Japan
[2]Research Center for Advanced Science and Technology, The University of Tokyo, Tokyo, Japan
[3]Woods Hole Oceanographic Institution, Woods Hole, MA, USA
[4]Faculty of Sustainable Design, University of Toyama, Toyama, Japan

Correspondence: Ayako Yamamoto (ayako.yamamoto@jamstec.go.jp)

Abstract. Although conventionally attributed to dry dynamics, increasing evidence points to a key role of moist dynamics in the formation and maintenance of blocking events. The source of moisture crucial for these processes, however, remains elusive. In this study, we identify the moisture sources responsible for latent heating associated with the wintertime Euro-Atlantic blocking events detected over 31 years (1979-2010). To this end, we track atmospheric particles backward in time from the blocking centres for a period of 10 days, using an offline Lagrangian dispersion model applied to an atmospheric reanalysis data.

The analysis reveals that 36 - 55% of particles gain a massive amount of heat and moisture from the ocean over the course of 10 days. Via large-scale ascent, these moist particles transport low potential vorticity (PV) air of low-altitude, low-latitude origins to the upper troposphere where the amplitude of blocking is the most prominent, consistent with the previous studies. PV of these moist particles remains significantly lower compared to their dry counterparts throughout the course of 10 days, preferentially constituting blocking cores.

Further analysis reveals that approximately two-thirds of the moist particles source their moisture locally from the Atlantic, while the remaining one-third from the Pacific. The Gulf Stream and Kuroshio and their extensions, as well as the eastern Pacific northeast of Hawaii, not only provide heat and moisture to the particles but also act as "springboards" for their large-scale, cross-isentropic ascent. While the particles of the Atlantic origin swiftly ascend just before their arrival at the blocking, those of the Pacific origin ascend additional few days earlier, after which they carry low PV in the same manner as dry particles. Thus, our study reveals that what may appear to be a blocking maintenance mechanism governed by dry dynamics alone can, in fact, be of moist origin.

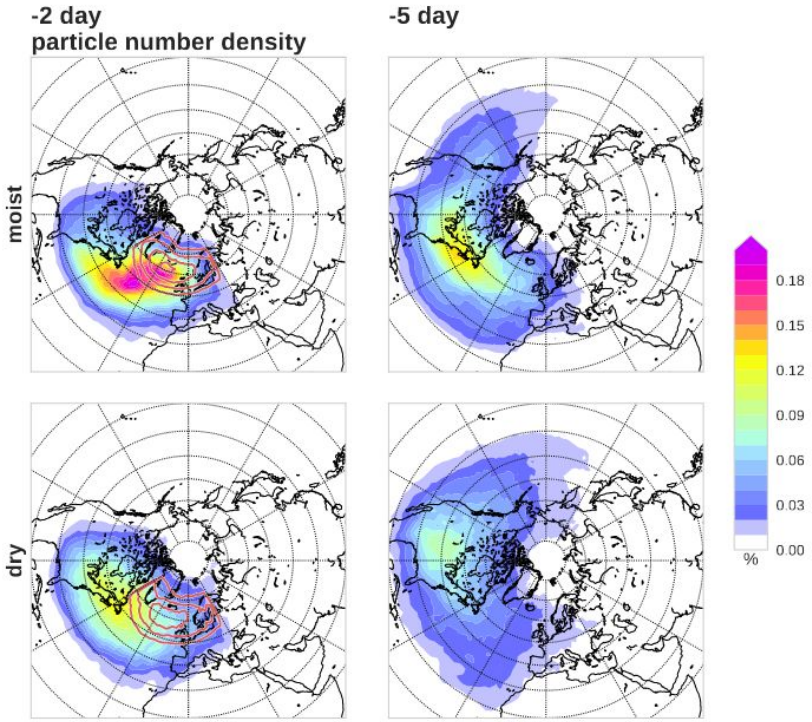

Number density for each 2°×2° grid cell for the moist particles (top) and dry particles (bottom) 2 days (left column), 5 days(middle column), and 9 days (right column) prior to their arrival at the wintertime Euro-Atlantic blocking highs. Red contours denote the location of the particle release location (i.e. where the blocks form) with the interval of 0.05% starting from 0.1%. In each panel the sum ofall grid cells is 100%.

Yamamoto et al., 2020.

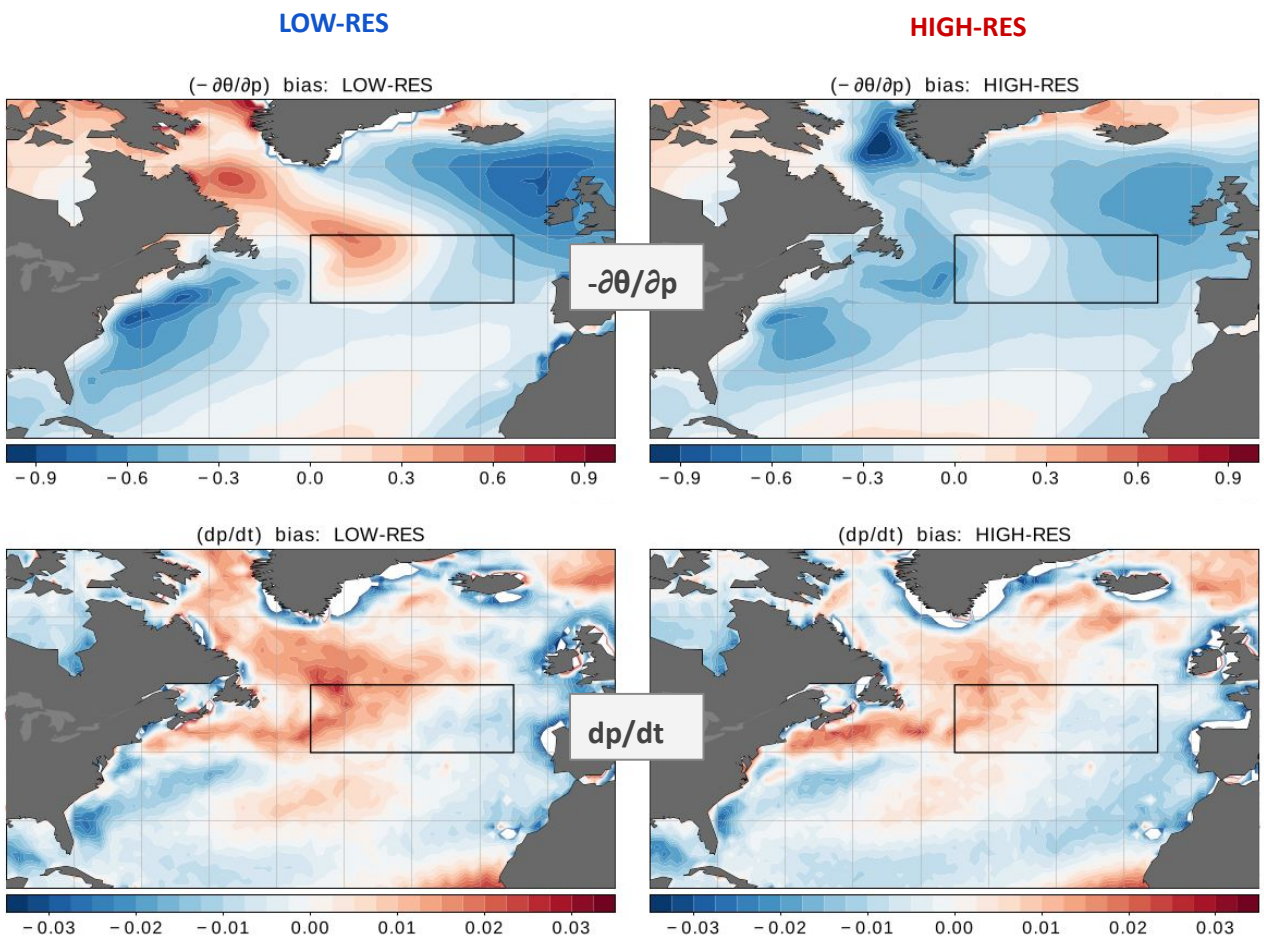

Biases in static stability $(-\partial\theta/\partial p)$ at 850 hPa in K $(100\ \text{hPa})^{-1}$
and in vertical velocity (dp/dt) at 700 hPa in Pa s^{-1}.

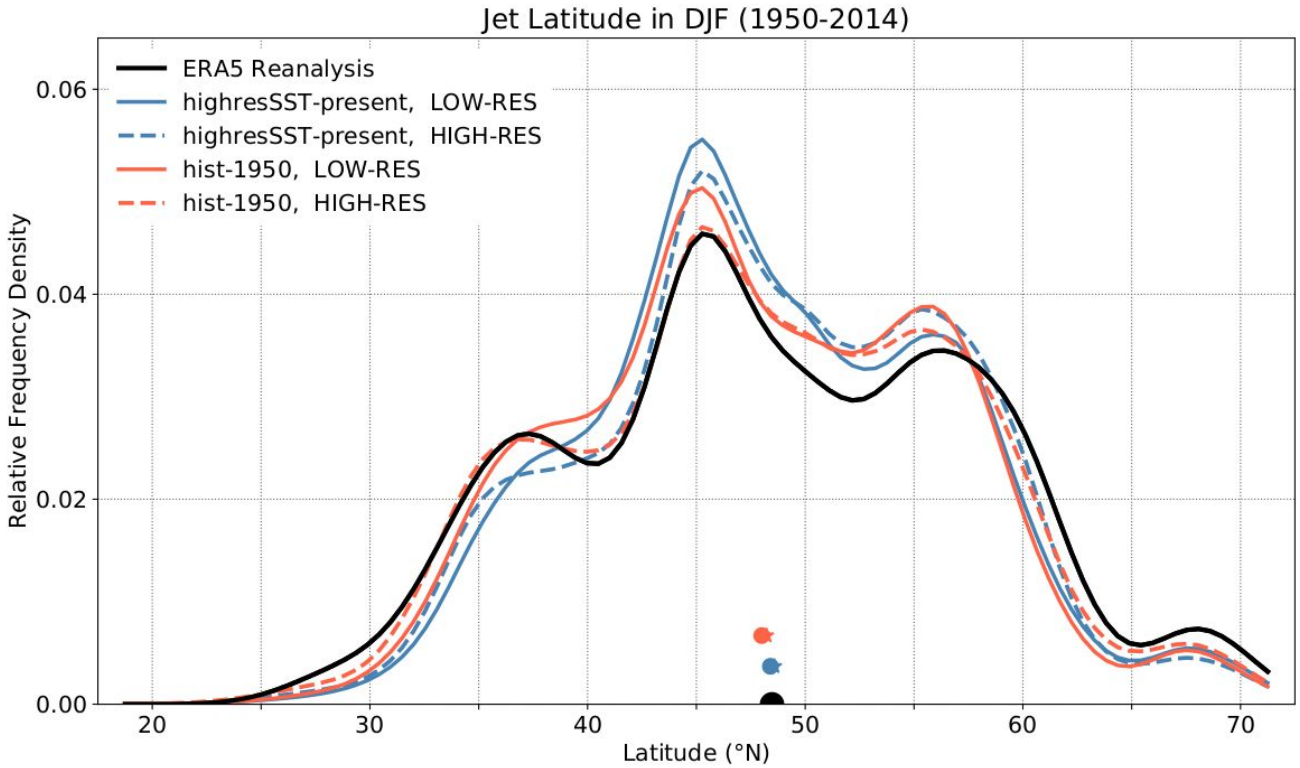

North Atlantic jet-latitude distributions. The horizontal position of the markers shows the respective mean values. Round markers and solid lines for LOW-RES, asterisks and dashed lines for HIGH-RES. Blue lines and markers are for the atmosphere-only historical simulations (*highresSST-present*), while red lines and markers are for the coupled historical simulations (*hist-1950*). The black line and marker correspond to the ERA5 reanalysis for the same period.

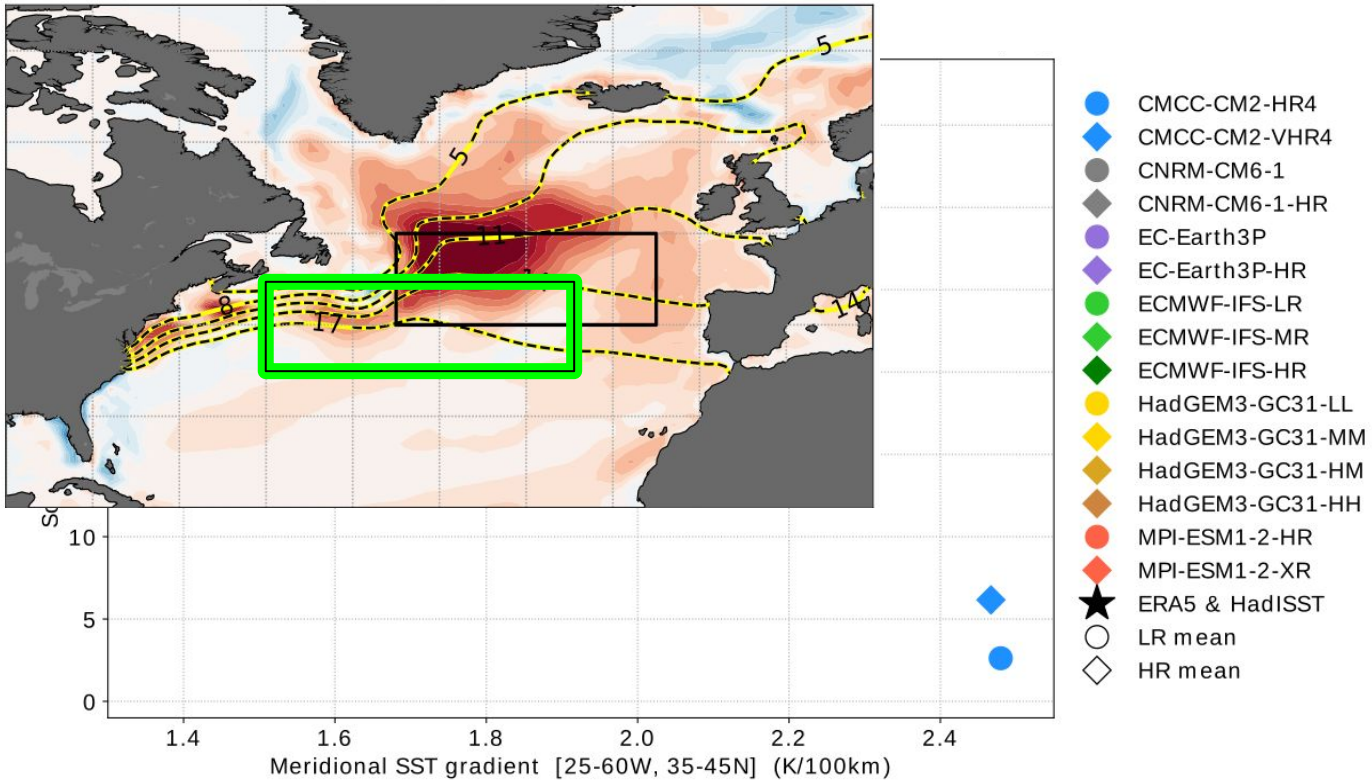

Figure 8: Climatological frequency (% of days) of the southern-jet regime (jet latitude < 38°N) in wintertime for each model vs the respective climatological meridional SST gradient in the area [25°–60°W, 35°–45°N]. Round markers are for LR models, diamond markers are for HR models, while the black asterisks indicate the respective observations.

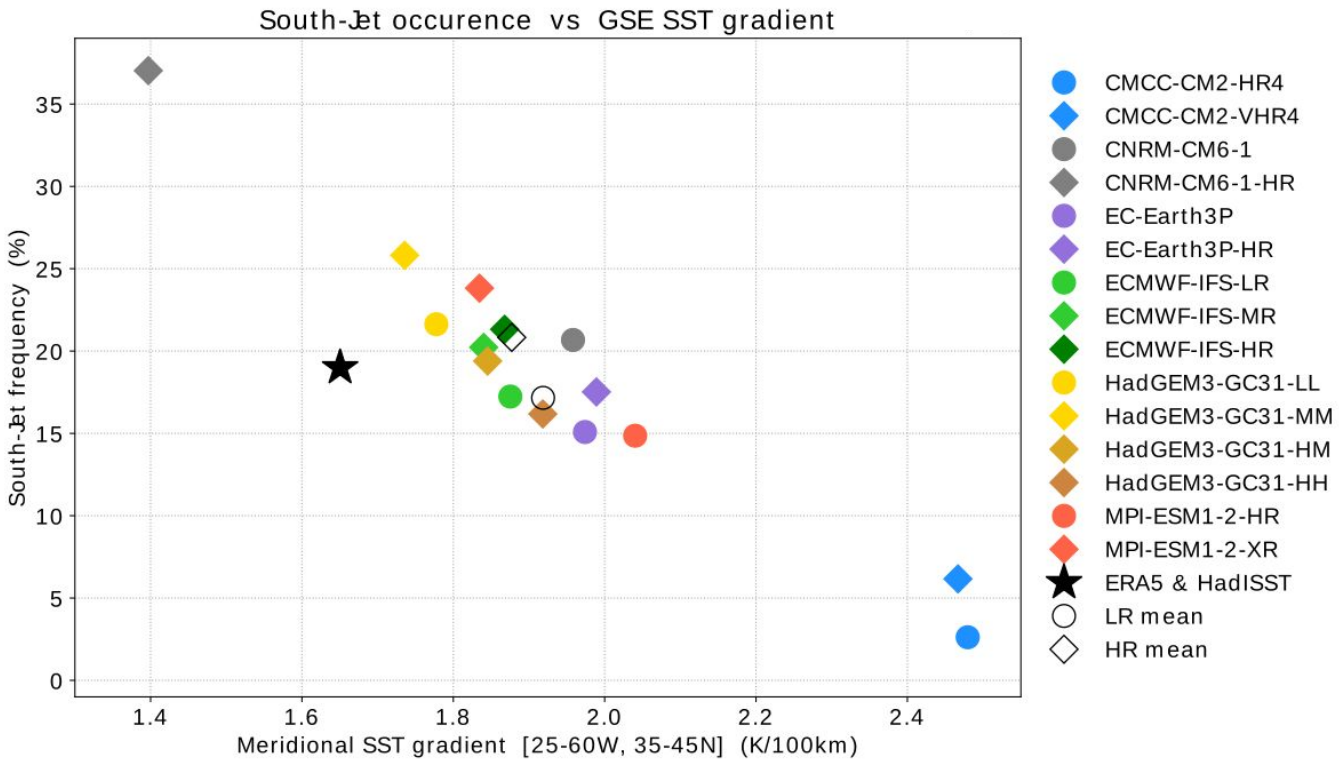

Figure 8: Climatological frequency (% of days) of the southern-jet regime (jet latitude < 38°N) in wintertime for each model vs the respective climatological meridional SST gradient in the area [25°–60°W, 35°–45°N]. Round markers are for LR models, diamond markers are for HR models, while the black asterisks indicate the respective observations.

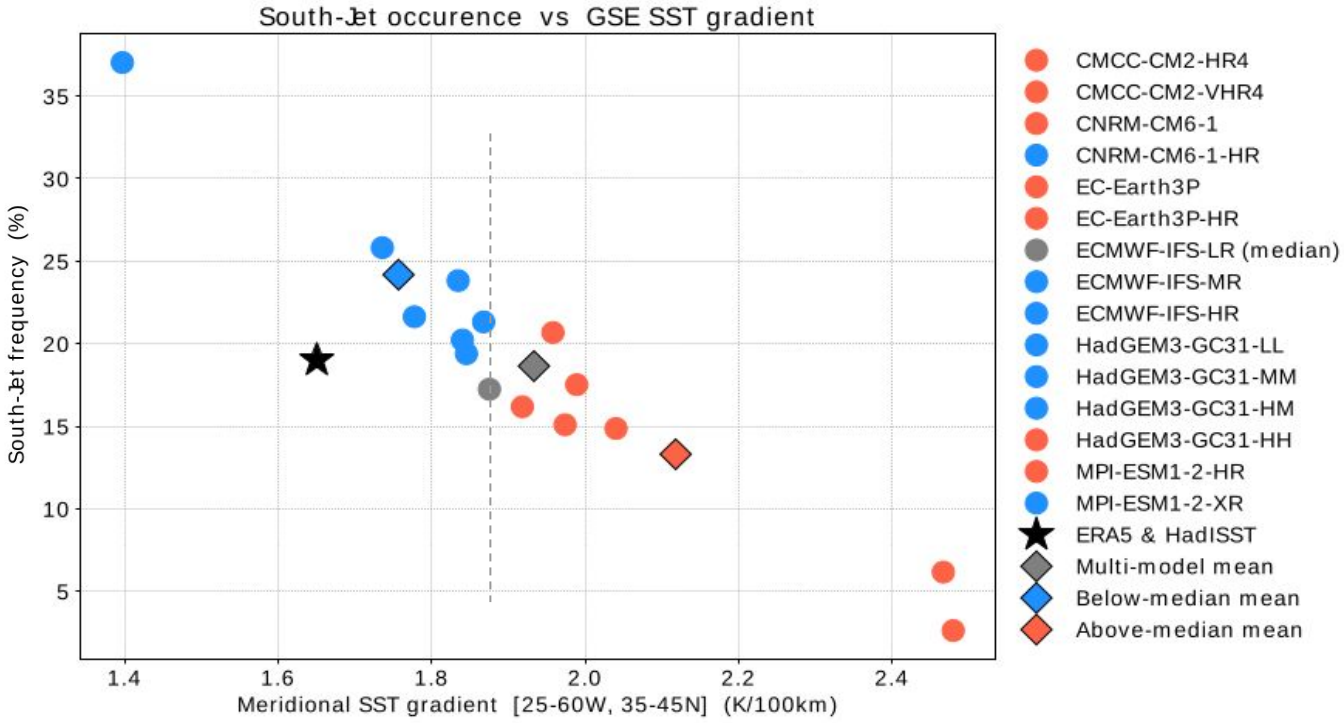

Figure S8: The multi-model ensemble partitioned to High-Grad **(red)** and Low-Grad **(blue)** sub-ensembles defined via the median climatological maximum SST gradient in the indicated area (two groups of colored markers and the respective means).

Comparing sub-ensemble climatologies

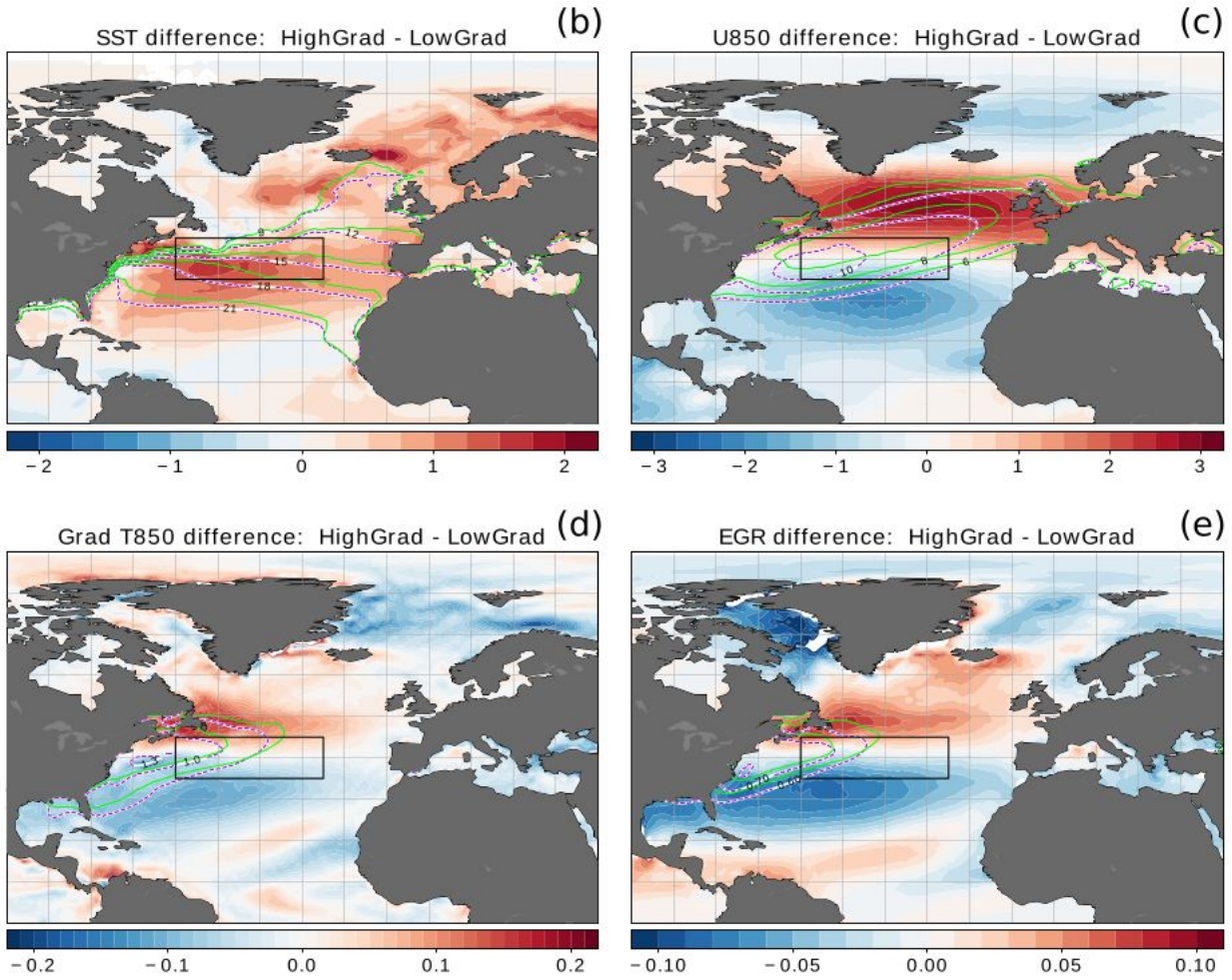

Figure S8: The panels show the differences between the two sub-ensemble means in terms of: (b) SST in °C with the respective climatologies in contours, solid green for High-Grad and dashed violet for Low-Grad, (c) zonal wind at 850 hPa, in m s^{-1}, (d) meridional gradient of air-temperature at 850 hPa, gradients are considered to be positive equatorward, in K (100 km)$^{-1}$, and (e) maximum Eady growth rate at 775 hPa, in day^{-1}.

Conclusions

- SST biases in the central North Atlantic, as evaluated in PRIMAVERA HighResMIP historical simulations, get significantly reduced with increasing oceanic resolution.

Conclusions

- SST biases in the central North Atlantic, as evaluated in PRIMAVERA HighResMIP historical simulations, get significantly reduced with increasing oceanic resolution.

- The same is true for biases in European blocking (its underestimation is improved) affecting also the climatology and variability of the eddy-driven jet and stormtrack.

Conclusions

- SST biases in the central North Atlantic, as evaluated in PRIMAVERA HighResMIP historical simulations, get significantly reduced with increasing oceanic resolution.
- The same is true for biases in European blocking (its underestimation is improved) affecting also the climatology and variability of the eddy-driven jet and stormtrack.
- A causal chain was identified: cold SST biases → higher SST gradients → higher low-level baroclinicity → biases in baroclinic activity → biases in eddy–mean flow interaction → biases in eddy-driven jet and European blocking.

Conclusions

- SST biases in the central North Atlantic, as evaluated in PRIMAVERA HighResMIP historical simulations, get significantly reduced with increasing oceanic resolution.
- The same is true for biases in European blocking (its underestimation is improved) affecting also the climatology and variability of the eddy-driven jet and stormtrack.
- A causal chain was identified: cold SST biases → higher SST gradients → higher low-level baroclinicity → biases in baroclinic activity → biases in eddy–mean flow interaction → biases in eddy-driven jet and European blocking.
- Regarding SST biases at the beginning of the NAC, it was shown that severe cold biases exhibited by most low-resolution models lead to equally severe biases in surface turbulent heat fluxes, strongly affecting stability, vertical motion and precipitation (diabatic heating) in that area.

Conclusions

- SST biases in the central North Atlantic, as evaluated in PRIMAVERA HighResMIP historical simulations, get significantly reduced with increasing oceanic resolution.
- The same is true for biases in European blocking (its underestimation is improved) affecting also the climatology and variability of the eddy-driven jet and stormtrack.
- A causal chain was identified: cold SST biases → higher SST gradients → higher low-level baroclinicity → biases in baroclinic activity → biases in eddy–mean flow interaction → biases in eddy-driven jet and European blocking.
- Regarding SST biases at the beginning of the NAC, it was shown that severe cold biases exhibited by most low-resolution models lead to equally severe biases in surface turbulent heat fluxes, strongly affecting stability, vertical motion and precipitation (diabatic heating) in that area.
- The magnitude of the time-mean meridional SST gradient at the central North Atlantic determines the time-mean low-level baroclinicity in that area; the same holds for the respective decadal variations.

Conclusions

- SST biases in the central North Atlantic, as evaluated in PRIMAVERA HighResMIP historical simulations, get significantly reduced with increasing oceanic resolution.
- The same is true for biases in European blocking (its underestimation is improved) affecting also the climatology and variability of the eddy-driven jet and stormtrack.
- A causal chain was identified: cold SST biases → higher SST gradients → higher low-level baroclinicity → biases in baroclinic activity → biases in eddy–mean flow interaction → biases in eddy-driven jet and European blocking.
- Regarding SST biases at the beginning of the NAC, it was shown that severe cold biases exhibited by most low-resolution models lead to equally severe biases in surface turbulent heat fluxes, strongly affecting stability, vertical motion and precipitation (diabatic heating) in that area.
- The magnitude of the time-mean meridional SST gradient at the central North Atlantic determines the time-mean low-level baroclinicity in that area; the same holds for the respective decadal variations.
- A relationship was found between biases in the maximum meridional SST gradient along the GSE and farther downstream and biases in high-latitude blocking and the southern-jet occurrence.

Conclusions

- SST biases in the central North Atlantic, as evaluated in PRIMAVERA HighResMIP historical simulations, get significantly reduced with increasing oceanic resolution.
- The same is true for biases in European blocking (its underestimation is improved) affecting also the climatology and variability of the eddy-driven jet and stormtrack.
- A causal chain was identified: cold SST biases → higher SST gradients → higher low-level baroclinicity → biases in baroclinic activity → biases in eddy–mean flow interaction → biases in eddy-driven jet and European blocking.
- Regarding SST biases at the beginning of the NAC, it was shown that severe cold biases exhibited by most low-resolution models lead to equally severe biases in surface turbulent heat fluxes, strongly affecting stability, vertical motion and precipitation (diabatic heating) in that area.
- The magnitude of the time-mean meridional SST gradient at the central North Atlantic determines the time-mean low-level baroclinicity in that area; the same holds for the respective decadal variations.
- A relationship was found between biases in the maximum meridional SST gradient along the GSE and farther downstream and biases in high-latitude blocking and the southern-jet occurrence.

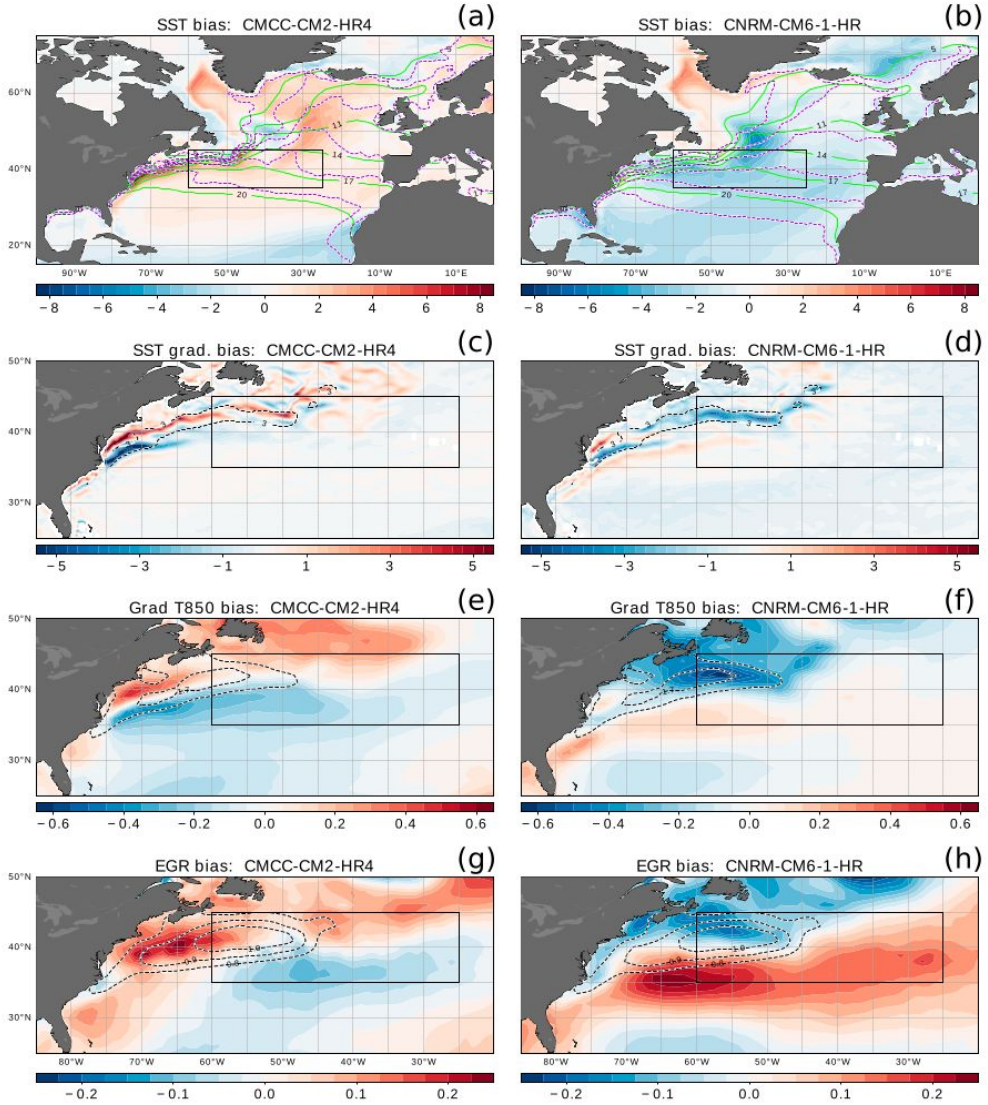

FIG. 9. Comparison of biases for the "outlier" models (CMCC-CM2-HR4 and CNRM-CM6-1-HR) seen in the previous figure. (a),(b) SST biases (K), with solid green contours for the observed climatology and dashed violet contours for the respective model climatology, (c),(d) biases in meridional SST gradient [K (100 km)$^{-1}$], (e),(f) biases in meridional gradient of air temperature at 850 hPa [K (100 km)$^{-1}$], and (g),(h) biases in maximum Eady growth rate at about 885 hPa (day^{-1}). Dashed black contours refer to the respective observed climatology in the same season (DJF) and period (1950–2014). All rectangular frames correspond to 25°–60°W, 35°–45°N.

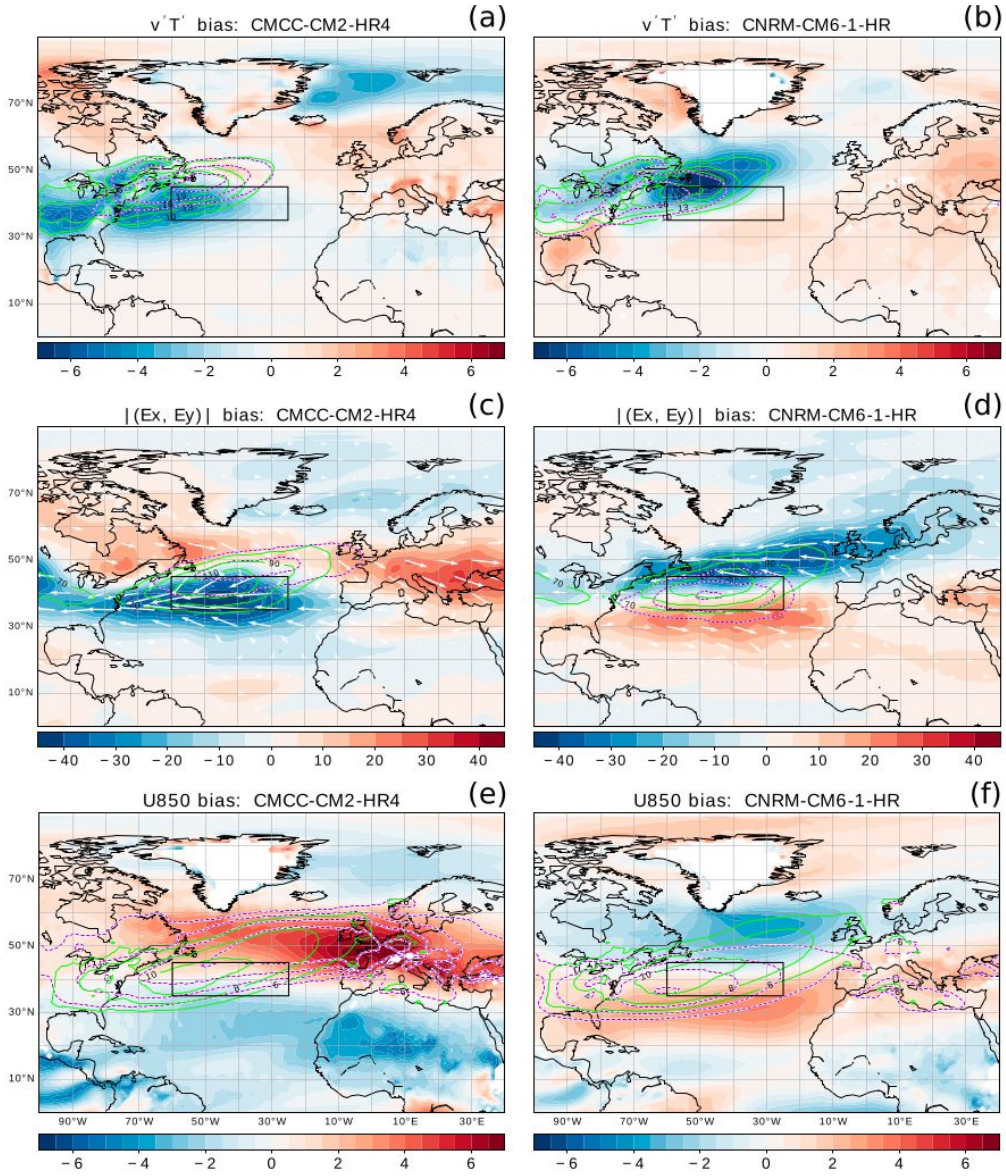

FIG. 10. As in Fig. 9, but showing (a),(b) biases in baroclinic eddy fluxes ($v'T'$) at 850 hPa (K m s^{-1}), (c),(c) biases in the magnitude of the horizontal E-vector ($\overline{v'^2 - u'^2}$, $\overline{-u'v'}$) at 250 hPa (m^2 s^{-2}, with the arrows showing biases in the respective components), and (e),(f) biases in zonal wind at 850 hPa (m s^{-1}). As in Fig. 6, primes denote high-pass filtering of daily data (details in the text). All rectangular frames correspond to 25°–60°W, 35°–45°N, as in Fig. 9.

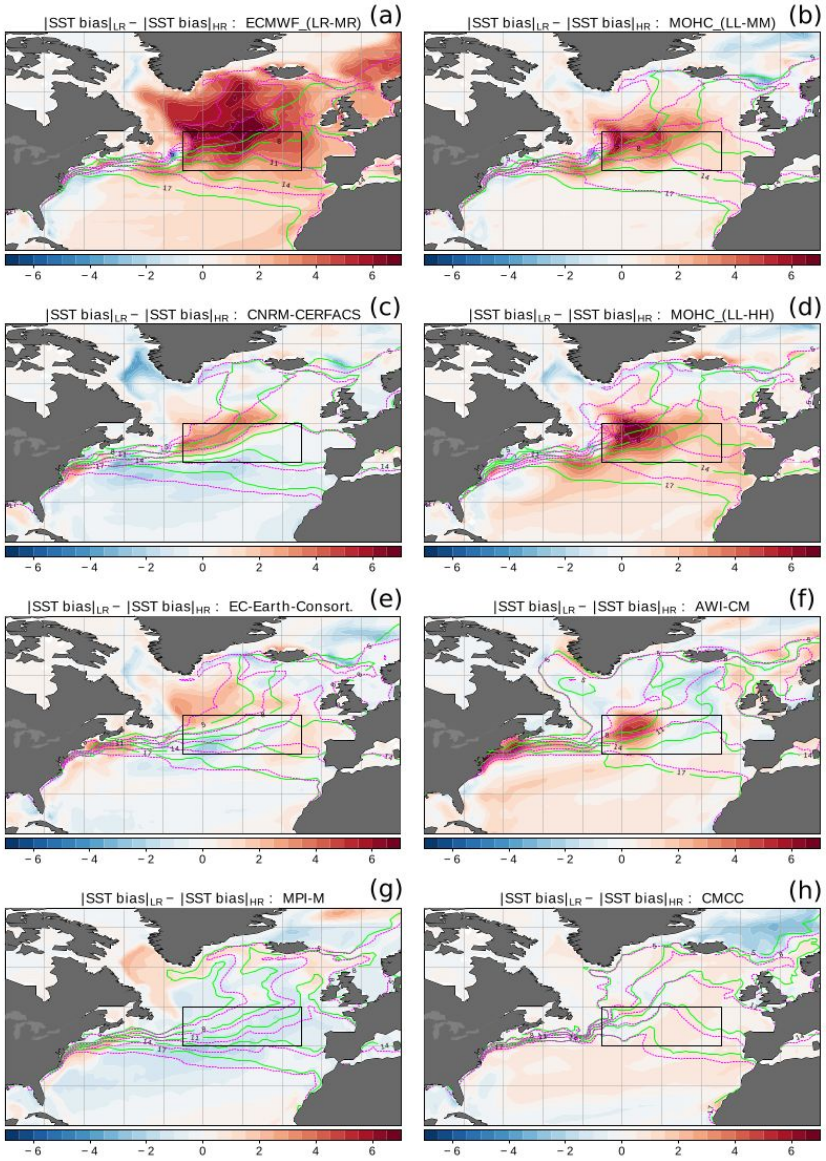

FIG. 2. Differences in absolute SST bias between "LR" and "HR" model pairs (Table 1). Climatological isotherms are shown in contours, solid green for "LR" models and dashed violet for "HR" models. The rectangular frame defines the area of interest (referred to as Central North Atlantic in the text) where the model biases modify the climatological meridional SST gradient. The bottom panels correspond to the models (CMCC and MPI-M) that increase only the atmospheric resolution.

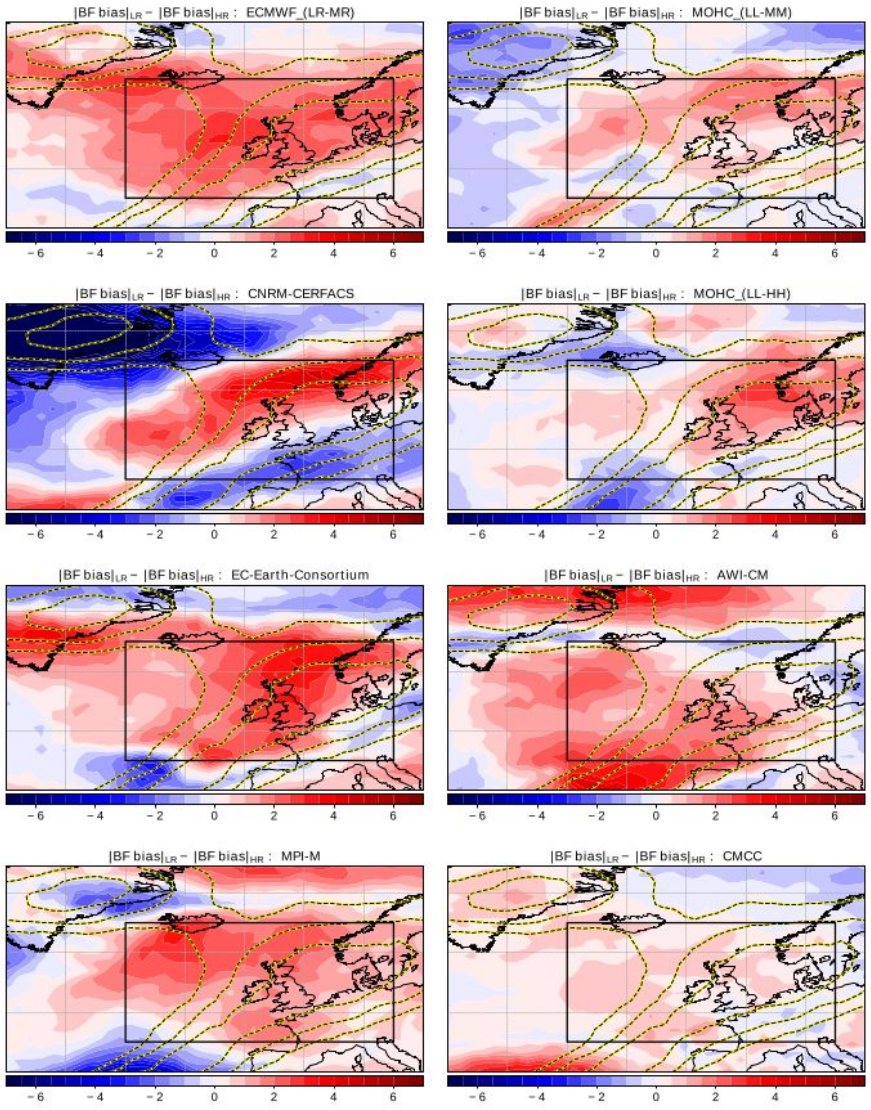

Figure S1: Differences in wintertime absolute blocking frequency bias between "LR" and "HR" model pairs (Table 1). Selected isolines of observed climatological blocking frequency are shown in contours (as in Fig. 1). The rectangular frame defines the area of interest where blocking frequency biases are generally reduced with increasing model resolution.

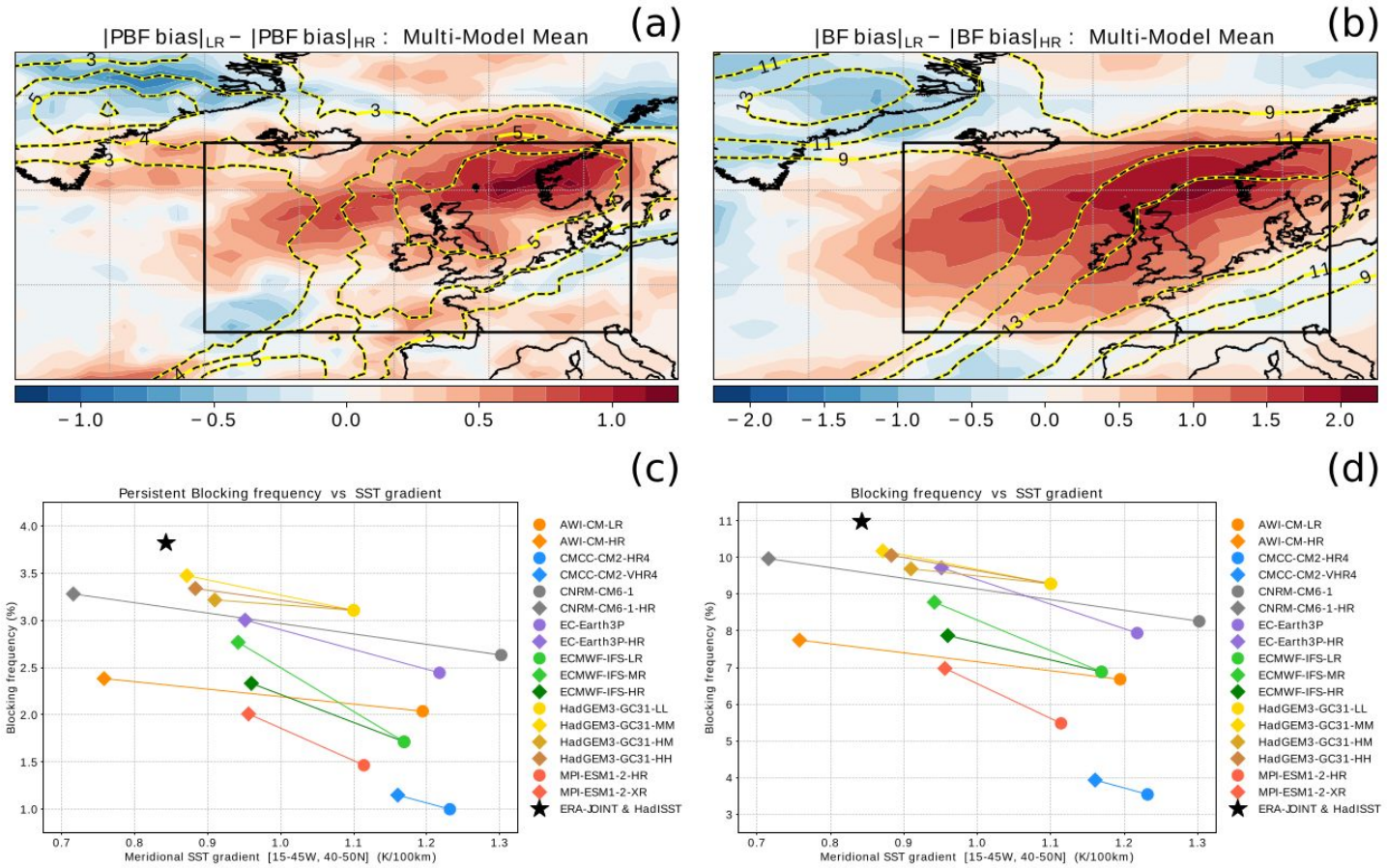

Figure S2: Comparing results for blocking with (left) and without (right) a 5-day persistence criterion applied. The right-hand-side panels are reproduced from Fig. 1 and Fig. 4 and are shown here only to aid the comparison. Other details as in the respective figures.

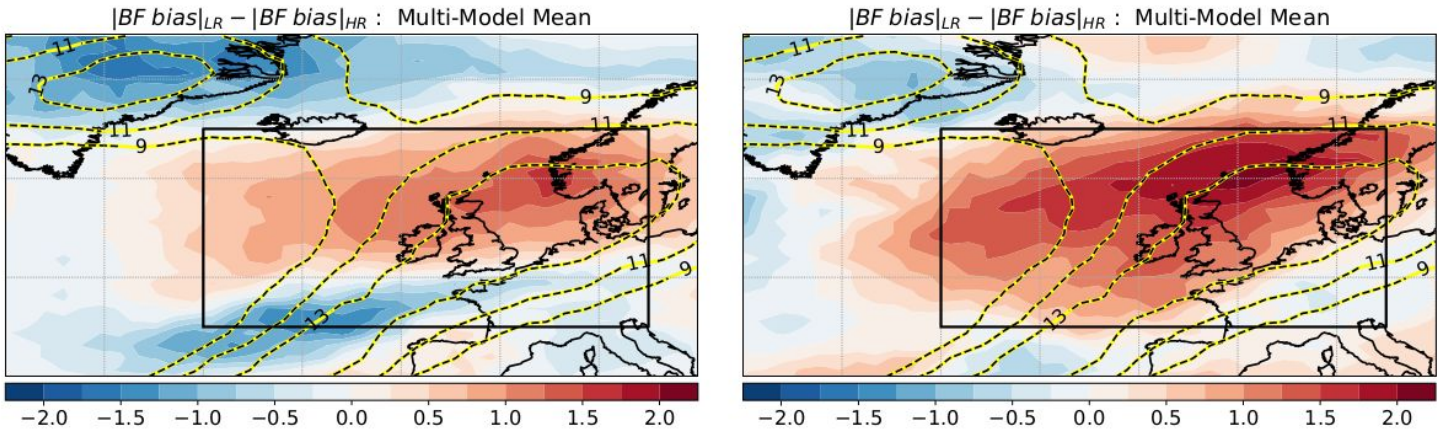

Figure S6: Comparison of multi-model bias reduction in blocking frequency with increasing resolution between coupled historical simulations "hist-1950" on the right (reproduced from Fig. 1) and the respective atmosphere-only forced historical simulations "highresSST-present" on the left. Other details as in Fig. 1b.

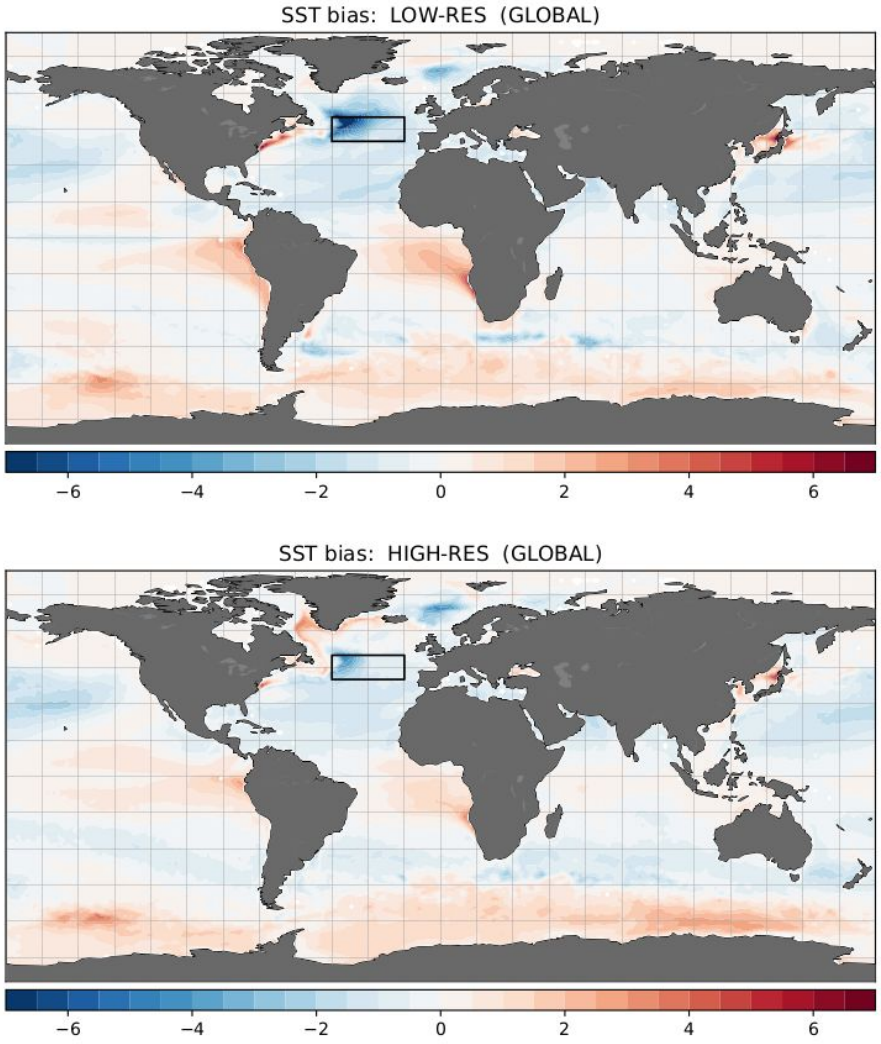

Figure S7: Multi-model mean SST biases in wintertime with respect to HadISST2 for the LOW-RES (top) and HIGH-RES (bottom) sub-ensembles as indicated in Table 1, in K. The rectangular frames correspond to [15–45°W, 40–50°N], as in Fig. 5.

For the computation of the horizontal E-vector components $(\overline{u'^2 - \nu'^2},\ \overline{u'\nu'})$ and the meridional eddy heat flux $(\overline{\nu'T'})$, high-frequency transients (denoted by a prime) were defined via a high-pass Lanczos filter retaining periods lower than 10 days, as in Novak et al. (2015). Following Hoskins et al. (1983), these two variables are used to assess the impact of baroclinic eddies on the mean westerly flow. The atmo-

The maximum Eady growth rate is computed as $\sigma = 0.31 \frac{f}{N} \frac{\partial U}{\partial Z}$, where f is the Coriolis parameter, N is the static stability parameter [as in James (1994)], Z is the geopotential height and $U = \sqrt{u^2 + \nu^2}$ is the magnitude of the horizontal wind. The vertical derivative is computed between the 850 hPa and 700 hPa isobaric levels. Regarding EGR climatologies, using monthly mean instead of daily mean data was found to make no significant difference.

Finally, horizontal gradients of SST and air-temperature at 850 hPa were computed on the sphere using central differences scheme on the sphere.

Climate Dynamics (2018) 51:3369–3387
https://doi.org/10.1007/s00382-018-4083-9

Impact of Gulf Stream SST biases on the global atmospheric circulation

Robert W. Lee[1] · Tim J. Woollings[2] · Brian J. Hoskins[3] · Keith D. Williams[4] · Christopher H. O'Reilly[2] · Giacomo Masato[1]

Received: 12 July 2017 / Accepted: 11 January 2018 / Published online: 7 February 2018

Yet, the 60-km atmospheric resolution was probably insufficient for simulating a realistic response to the imposed SST anomalies.

Abstract

The UK Met Office Unified Model in the Global Coupled 2 (GC2) configuration has a warm bias of up to almost 7 K in the Gulf Stream SSTs in the winter season, which is associated with surface heat flux biases and potentially related to biases in the atmospheric circulation. The role of this SST bias is examined with a focus on the tropospheric response by performing three sensitivity experiments. The SST biases are imposed on the atmosphere-only configuration of the model over a small and medium section of the Gulf Stream, and also the wider North Atlantic. Here we show that the dynamical response to this anomalous Gulf Stream heating (and associated shifting and changing SST gradients) is to enhance vertical motion in the transient eddies over the Gulf Stream, rather than balance the heating with a linear dynamical meridional wind or meridional eddy heat transport. Together with the imposed Gulf Stream heating bias, the response affects the troposphere not only locally but also in remote regions of the Northern Hemisphere via a planetary Rossby wave response. The sensitivity experiments partially reproduce some of the differences in the coupled configuration of the model relative to the atmosphere-only configuration and to the ERA-Interim reanalysis. These biases may have implications for the ability of the model to respond correctly to variability or changes in the Gulf Stream. Better global prediction therefore requires particular focus on reducing any large western boundary current SST biases in these regions of high ocean-atmosphere interaction.

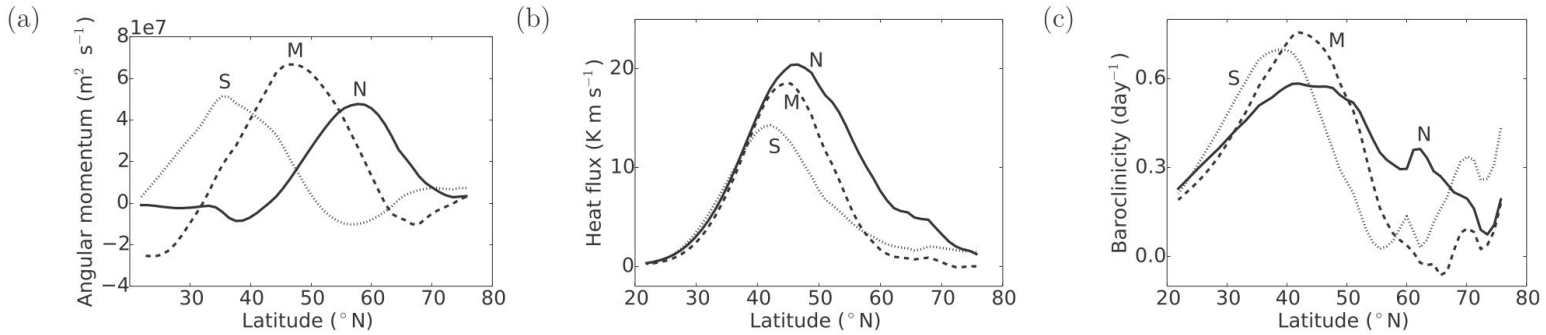

FIG. 2. Composites of latitudinal profiles of the (a) lower-level relative angular momentum ($m^2 s^{-1}$; averaged between 0° and 30°W), (b) heat flux (K m s^{-1}; averaged between 40° and 70°W), and (c) baroclinicity (day^{-1}; averaged between 30° and 90°W) for the S (dotted), M (dashed), and N (solid) regimes.

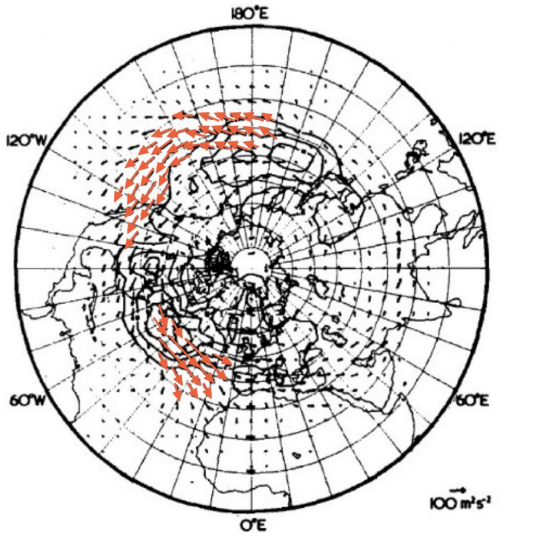

Contours show poleward heat flux $\overline{v'T'}$ at 700 hPa and arrows show $(\overline{v'^2} - \overline{u'^2}, -\overline{v'u'})$ at 250 hPa for synoptic (high-pass) eddies. Data for N. hemisphere winter 1979–80. Contour interval is 5 K m s^{-1}.

Hosking et al. (1983)

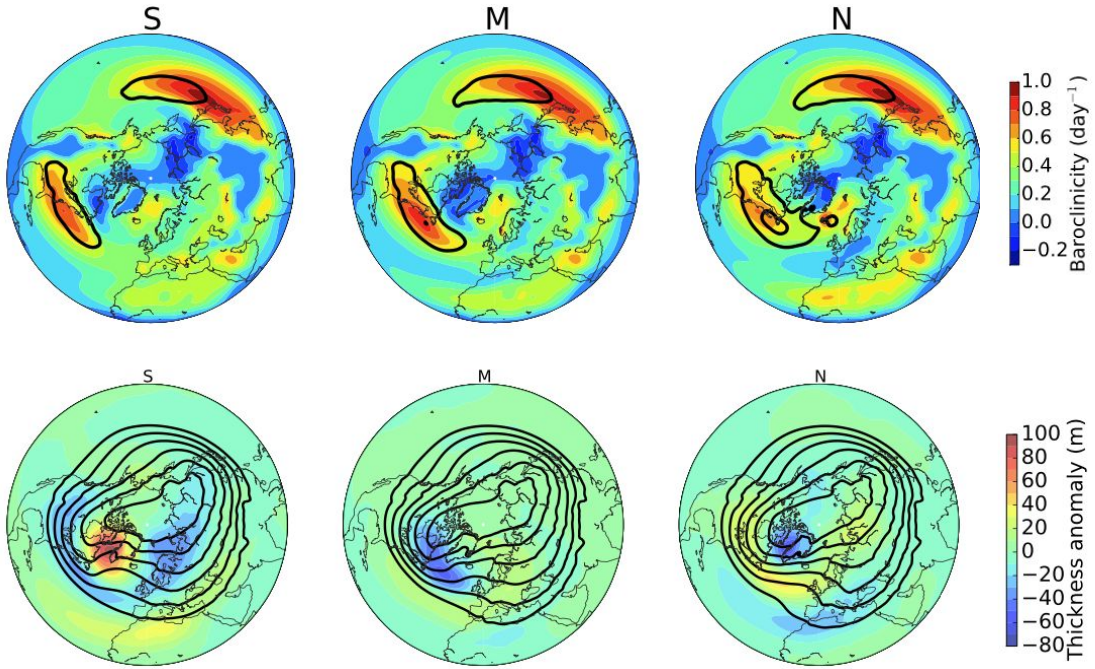

Novak et al. (2015)

The atmospheric frontal response to SST perturbations in the Gulf Stream region

Rhys Parfitt[1], Arnaud Czaja[1], Shoshiro Minobe[2], and Akira Kuwano-Yoshida[3]

[1]Department of Physics, Imperial College London, London, UK, [2]Department of Natural History Sciences, Graduate School of Science, Hokkaido University, Sapporo, Japan, [3]Application Laboratory, Japan Agency for Marine-Earth Science and Technology, Yokohama, Japan

Abstract The link between sea surface temperature (SST) gradients and atmospheric fronts is explored in a general circulation model across the Gulf Stream (GS) region from December to February 1981–2000. Two model experiments are analyzed, one with a realistic control SST distribution and one with a spatially smoothed SST distribution. The analysis shows a noticeable change in regional atmospheric frontal frequency between the two experiments (up to 30%), with the distribution of change exhibiting a clear imprint of the GS SST front. Further analysis of the surface sensible heat flux gradient across cold fronts reveals the pattern of change to be mediated by a thermal interaction between the oceanic and atmospheric fronts ("thermal damping and strengthening"). These results not only emphasize the significance of the GS SST gradient for storm development in the North Atlantic but also highlight the importance of resolution in assessing the role of frontal air-sea interaction in midlatitude climate variability.

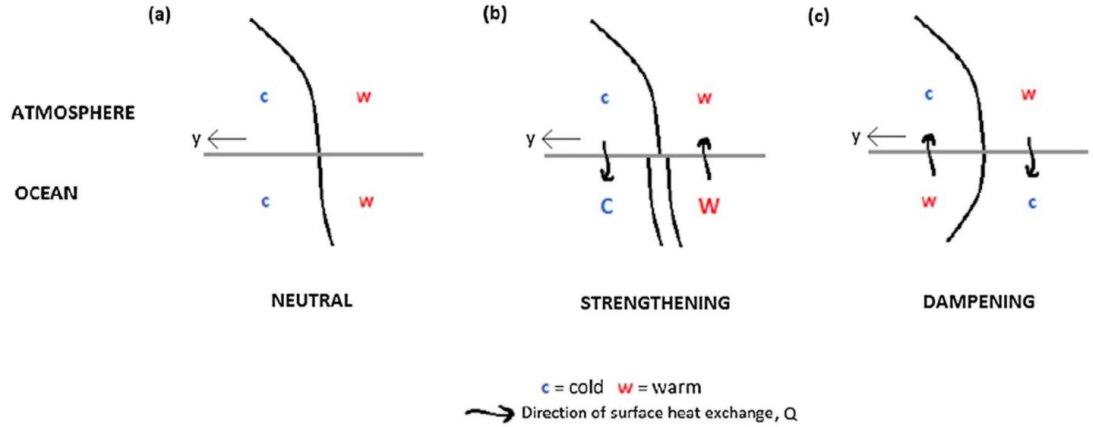

Figure 4. Schematic of an atmospheric cold front passing over (a) an SST gradient aligned such that the ocean temperature is equal to the atmospheric temperature at the surface, (b) a strong SST gradient aligned in the same direction, and (c) an SST gradient aligned in the opposite direction. Black wavy arrows indicate the direction of surface sensible heat fluxes, while the cross-frontal direction vector (y) is shown as a thin black arrow (positive toward the cold sector).

Importance of latent heat release in ascending air streams for atmospheric blocking

S. Pfahl ✉, C. Schwierz, M. Croci-Maspoli, C. M. Grams & H. Wernli

Nature Geoscience **8**, 610–614 (2015) | Cite this article

Abstract

Atmospheric blocking is a key component of extratropical weather variability[1] and can contribute to various types of extreme weather events[2,3,4,5]. Changes in blocking frequencies due to Arctic amplification and sea ice loss may enhance extreme events[6,7], but the mechanisms potentially involved in such changes are under discussion[8,9,10,11]. Current theories for blocking are essentially based on dry dynamics and do not directly take moist processes into account[12,13,14,15,16,17]. Here we analyse a 21-year climatology of blocking from reanalysis data with a Lagrangian approach, to quantify the release of latent heat in clouds along the trajectories that enter the blocking systems. We show that 30 to 45% of the air masses involved in Northern Hemisphere blocking are heated by more than 2 K—with a median heating of more than 7 K—in the three days before their arrival in the blocking system. This number increases to 60 to 70% when considering a seven-day period. Our analysis reveals that, in addition to quasi-horizontal advection of air with low potential vorticity[12,13,14,15], ascent from lower levels associated with latent heating in clouds is of first-order importance for the formation and maintenance of blocking. We suggest that this process should be accounted for when investigating future changes in atmospheric blocking.

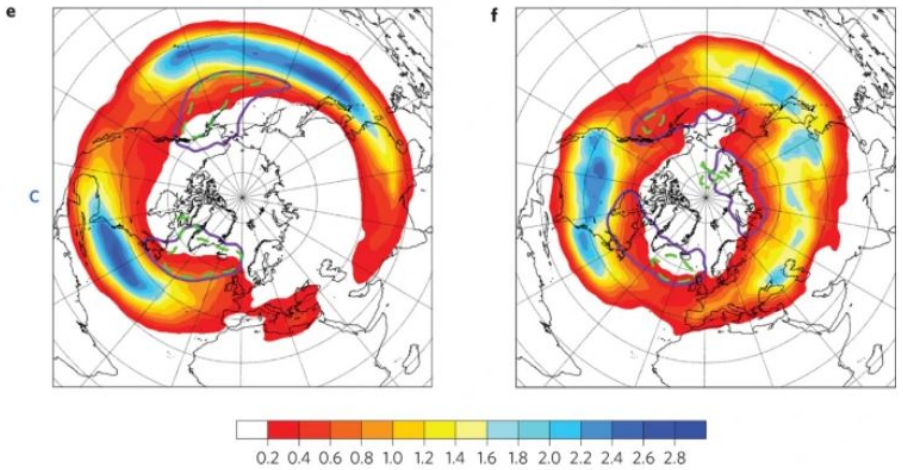

Colour shading shows spatial densities of air parcels three days before arriving in a blocking region for the three categories defined in Fig. 1a (**a**,**b**: category A; **c**,**d**: category B; **e**,**f**: category C) over the winter (left column) and summer season (right column). Units are % $(10^6\ \mathrm{km})^{-1}$ and are normalized such that the spatial integral over each distribution yields 1. The purple contours indicate the main backward trajectory starting locations (density contour value of 2; see Supplementary Fig. 9). Regions where the total blocking frequency is larger than 7% are shown by the dashed green contours.